ELSEVIER

Lithos 61 (2002) 21–53

LITHOS

www.elsevier.com/locate/lithos

B_1 basaltic lavas in Vestfold–Jeløya area, central Oslo rift: derivation from initial melts formed by progressive partial melting of an enriched mantle source

E.-R. Neumann [a,*], E.A. Dunworth [b], B.A. Sundvoll [b], J.I. Tollefsrud [b,1]

[a] *Department of Geology, the University of Oslo, P.O.Box 1047 Blindern, N-0316 Oslo, Norway*
[b] *Mineralogisk-geologisk museum, University of Oslo, Sarsgaten 1, N-0562 Oslo, Norway*

Received 12 December 2000; accepted 14 January 2002

Abstract

The earliest (B_1) lavas in Vestfold and Jeløya, in the central part of the Permo-Carboniferous Oslo rift have been divided into four main groups: high Ti (HT) basalts ($TiO_2 > 4.2$ wt.%), low Ti (LT) basaltic rocks ($TiO_2 < 3.7$ wt.%), phonotephrites and ignimbrites. They are all highly enriched in strongly incompatible elements and have high La/Yb ratios. Initial ε_{Nd} and ε_{Sr} ratios of whole-rock samples and clinopyroxene separates (assumed age = 295 Ma) are +6.0 to −1.6 and −17 to +57, respectively. Their trace element and isotopic compositions imply that, during ascent, the magmas were subjected to varying degrees of fractional crystallization, mixing between evolved and mafic magmas, and crustal contamination in the upper crust. Crustal contamination was most likely caused by rocks similar to the metasediments now exposed in the Bamble sector, south of the Oslo rift. The preserved lava sequences represent interfingering of lavas from at least three eruption centers. After extrusion, the lavas suffered post-magmatic alteration that led to mobilization of Rb, U and K, and increased $^{87}Sr/^{86}Sr$ ratios. Interpretation of magmatic signatures, inferred to have been preserved through contamination and alteration, allow us to make the following conclusions concerning the mantle sources of the Vestfold and Jeløya B_1 basalts. The formation of the HT-basalts involves highly Ti–P-rich, garnet-bearing mantle source rocks, e.g. clinopyroxenites, wehrlites, websterites, and amphibolites. The HT and LT basalts may have originated by progressive partial melting of a veined, enriched, garnet–phlogopite-bearing peridotite at the base of the lithosphere. Progressive melting of this complex source initially produced magnesian lavas with high REE and HFSE contents, followed by less enriched, more voluminous lavas. The early basalts were derived from an isotopically depleted source similar to the PREMA source. Contribution of older lithospheric material to the later basalts produced more enriched Sr–Nd isotopic signatures. As some of the most primitive basalts found within the European Permo-Carboniferous rifting event, these lavas are key to understanding the nature of the sublithospheric mantle beneath Europe at this time.

Keywords: Permo-Carboniferous; Europe; Oslo rift; Basalt; Mantle plume

1. Introduction

During the Permo-Carboniferous, the Variscan foreland in Europe was subjected to extensive rift-related

* Corresponding author. Tel.: +47-2285-6663.
E-mail address: e.r.neumann@geologi.uio.no (E.-R. Neumann).
[1] Present address: PGS Reservoir, P.O. Box 354, 1326 Lysaker, Norway.

0024-4937/02/$ - see front matter
PII: S0024-4937(02)00068-3

tectonism and related extensional magmatic activity. While the most voluminous, but evolved magmatism occurred in the North German Basin (Benek et al., 1996), the Oslo rift contains the most extensive and best preserved sequences of basaltic lavas associated with this large Permo-Carboniferous event.

Rb–Sr age determinations indicate that the total period of magmatic activity within the exposed segments of the Oslo rift lasted from about 305 to 245 Ma (Sundvoll et al., 1990), while the earliest basaltic magmatism appears to have been restricted to a relatively short period from about 305 to 290 Ma (Sund-

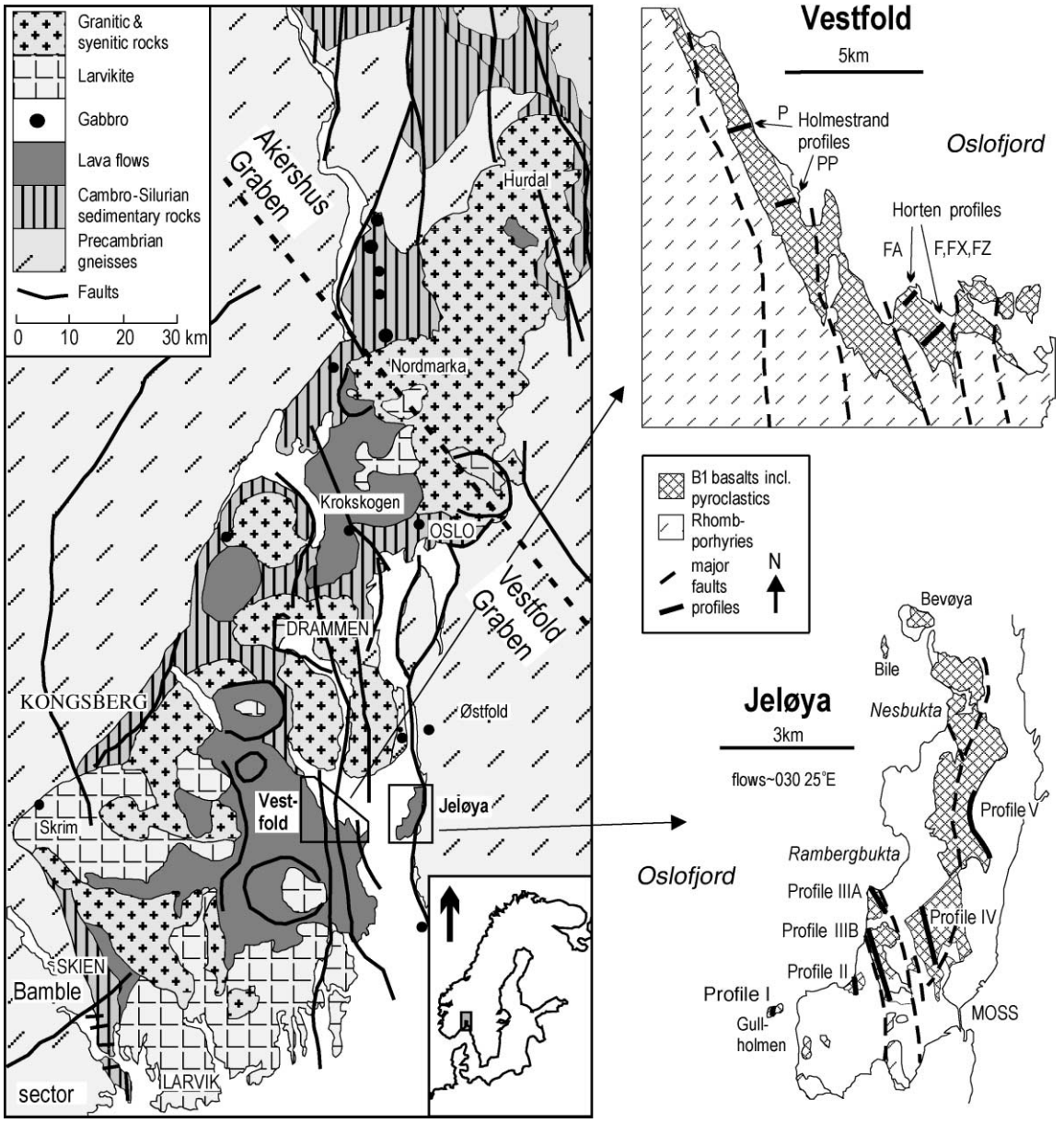

Fig. 1. Simplified geological map of the Oslo Region (based on map by Ramberg and Larsen, 1978) showing the location of the Vestfold and Jeløya B_1 sequences, and the relative positions of the profiles that have been sampled (insert).

Table 1
Previously unpublished major element compositions of B_1 lavas in Vestfold

Profile	B_1 Holmestrand S								B_1 Holmestrand N	
Sample	PP2a	PP3	PP4	PP5	PP6	PP7	PP8	P2	P3	P4
Type	HT	HT	LT	HT	LT	LT	HT	LT	LT	LT
SiO_2	44.71	44.88	47.01	43.62	45.78	48.06	45.87	44.72	47.01	48.12
TiO_2	4.22	4.78	2.25	5.20	3.55	2.77	5.00	3.73	3.41	2.87
Al_2O_3	9.23	9.55	9.15	7.46	13.49	12.91	10.12	7.77	8.20	12.76
$Fe_2O_{3\ total}$	14.34	14.60	13.61	16.41	15.15	13.86	14.96	16.01	14.99	12.75
MnO	0.20	0.22	0.30	0.18	0.21	0.19	0.15	0.22	0.21	0.15
MgO	10.85	11.34	13.16	11.95	7.18	7.85	8.09	12.77	10.29	7.53
CaO	13.31	10.98	14.13	12.97	10.11	10.98	11.48	13.86	12.07	11.11
Na_2O	1.58	1.73	0.90	0.94	2.76	2.54	2.23	1.02	1.81	2.53
K_2O	1.06	1.36	0.68	0.75	1.37	1.26	1.44	0.95	1.60	1.71
P_2O_5	0.46	0.56	0.19	0.53	0.41	0.37	0.66	0.51	0.42	0.45
TOTAL	99.96	100.00	101.38	100.01	100.01	100.79	100.00	101.56	100.01	99.98

Profile	B_1 Holmestrand N									
Sample	P5	P6	P7	P8	P8b	P9	P9a	P9b	P9c	P9d
Type	LT	LT	LT	LT	LT	LT	LT	LT	LT	LT
SiO_2	48.94	48.40	47.63	46.93	53.16	46.56	50.03	47.16	48.39	47.10
TiO_2	3.12	2.92	2.77	2.63	2.96	2.94	3.16	3.07	2.49	3.79
Al_2O_3	13.79	13.10	11.72	16.84	14.98	11.51	15.00	10.68	10.76	13.34
$Fe_2O_{3\ total}$	13.51	13.16	12.26	11.94	10.61	16.69	14.91	14.43	13.44	15.22
MnO	0.13	0.18	0.20	0.23	0.18	0.17	0.14	0.19	0.17	0.16
MgO	6.69	7.19	9.73	6.42	4.75	8.96	5.48	8.99	7.79	5.91
CaO	7.95	9.64	11.67	9.93	6.21	9.39	6.39	12.28	12.10	9.21
Na_2O	3.58	2.65	2.04	2.62	4.50	3.27	2.83	1.66	2.30	2.87
K_2O	1.83	2.32	1.59	2.03	2.21	0.39	1.64	1.14	2.23	1.86
P_2O_5	0.46	0.44	0.38	0.43	0.45	0.33	0.43	0.42	0.32	0.57
TOTAL	100.00	100.00	99.99	100.00	100.01	100.21	100.01	100.02	99.99	100.03

Profile	B_1 Holmestrand N							
Sample	P10	P12	P13	P14	P15	P16	P17	P18
Type	LT	LT	LT	LT	LT	LT	LT	LT
SiO_2	48.31	50.55	47.96	46.92	49.41	46.92	47.04	48.49
TiO_2	3.44	2.45	2.78	2.98	2.87	2.73	2.29	2.63
Al_2O_3	12.84	14.75	12.86	15.57	14.72	13.87	9.53	14.13
$Fe_2O_{3\ total}$	16.09	11.26	14.34	13.65	12.79	13.56	13.15	13.24
MnO	0.17	0.33	0.24	0.17	0.19	0.19	0.13	0.21
MgO	5.70	6.45	7.58	5.90	5.92	7.17	12.52	7.62
CaO	7.75	8.54	8.43	9.69	8.72	11.05	14.47	7.83
Na_2O	3.89	2.98	2.37	2.85	2.59	2.32	1.62	2.94
K_2O	1.33	2.09	3.02	1.93	2.25	1.77	0.33	2.50
P_2O_5	0.49	0.60	0.43	0.44	0.54	0.43	0.21	0.42
TOTAL	100.01	100.00	100.01	100.10	100.00	100.01	101.29	100.01

In each profile, the lavas are listed from bottom to top. For location of the profiles, see Fig. 1.

voll, unpublished data). These early basalts (B_1), including the Skien and Vestfold–Jeløya sequences, contain the least evolved magmatic products in the Oslo rift and are, thus, best suited to obtain information about the primary magmas and the magma sources involved in the magmatic activity.

No overview of the B_1 volcanism in the Vestfold–Jeløya area has so far been published. The aim of this

work is to present such an overview and to discuss the implications of lateral and time-related geochemical variations among the Vestfold–Jeløya B_1 volcanics with respect to: (a) magma chamber processes (crystallization, mixing, contamination); (b) the chemical character of the primary magmas; and (c) the chemical characteristics and origin of the mantle source. As a basis for discussion, we present new trace element and Sr–Nd isotopic data on sequences of B_1 volcanism in the area and integrate our results with those previously published.

2. Geological setting

The Permo-Carboniferous Oslo rift extends northwards from the Sorgenfrei–Tornquist Zone to Lake Mjøsa. It forms three opposing half-graben segments: the southern Skagerrak Graben, the central Vestfold graben, and the northern Akershus Graben (Fig. 1). Little is known about the magmatism in the submarine Skagerrak Graben; estimates based on seismic data suggest that a ~1-km-thick layer of lava was erupted (Heeremans, personal communication, 2000). The onshore part of the Oslo rift consists of a ~200-km-long and ~35–65-km-wide graben containing large volumes of rift-related extrusive and intrusive rocks, and minor amounts of rift-related sedimentary rocks, together with Cambro-Silurian sedimentary rocks, are preserved (Fig. 1). The Moho depth increases northwards from about 27 km near the Sorgenfrei–Torquist intersection to about 36 km in the lake Mjøsa area (Kinck et al., 1991). Furthermore, gravity and seismic data imply a different crustal structure along the rift than in the adjacent Precambrian terrain (e.g. Ramberg and Smithson, 1971; Ramberg, 1976; Wessel and Husebye, 1987; Kinck et al., 1991; Neumann et al., 1992). These differences include a smaller contrast in seismic velocities across the Moho inside than outside the rift and the existence of a "pillow" of dense material along the length of the Oslo rift; this pillow is most prominent in the Skien–Vestfold area (Fig. 1).

The eruptive activity in the Vestfold and Akershus graben segments appears to have progressed northwards (Sundvoll et al., 1990) with basaltic activity restricted to the central Vestfold Graben (Fig. 1). The "basalts" (nephelinites, tephrites, alkali basalts) are mainly concentrated in the lower part of the lava sequence, where they are known as the B_1 lavas. A 1500-m-thick sequence of mafic alkaline lavas occurs at Skien (Segalstad, 1979), a 170–180-m-thick sequence in Vestfold (Øverli, 1985; Tollefsrud, 1987), and a 800–1500-m-thick sequence in Jeløya (Schou-Jensen and Neumann, 1988). A single <30-m-thick B_1 tholeiite flow emplaced at the base of the Krokskogen lava sequence at the boundary between the Vestfold and Akershus graben segments (Ramberg and Larsen, 1978) is believed to be related to doleritic sill emplacement in western Sweden at this time (MacDonald et al., 1981). As well as the variations in thickness, the character of the B_1 lavas changes northwards from highly silica-undersaturated basaltic rocks in the Skien area (Fig. 1) through mildly silica-undersaturated to transitional compositions in the Vestfold–Jeløya area to quartz tholeiite at Krokskogen.

The magmatism subsequently continued with the extrusion of large volumes of rhomb porphyry lavas that may be described as latites (Le Maitre, 1989) or trachyandesites to tephriphonolites (Le Bas et al., 1986). These lie above the Vestfold–Jeløya and Krokskogen B_1 basalts and were interlayered with scattered basalt flows. The apparent lack of rhomb porphyry lavas above the main B_1 sequence in the

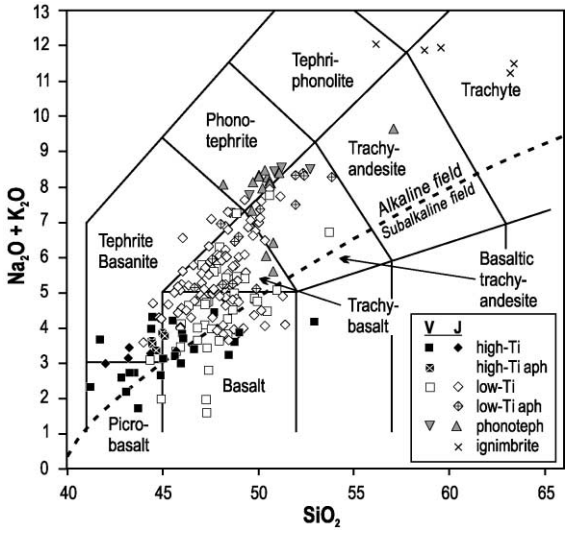

Fig. 2. $(K_2O + Na_2O)$–SiO_2 relations among the B_1 lavas in Vestfold and Jeløya. Classification is according to Le Bas et al. (1986). The alkaline–subalkaline division line is from Irvine and Baragar (1971). *V*: Vestfold; *J*: Jeløya; *aph*: aphyric; *phonoteph*: phonotephrites.

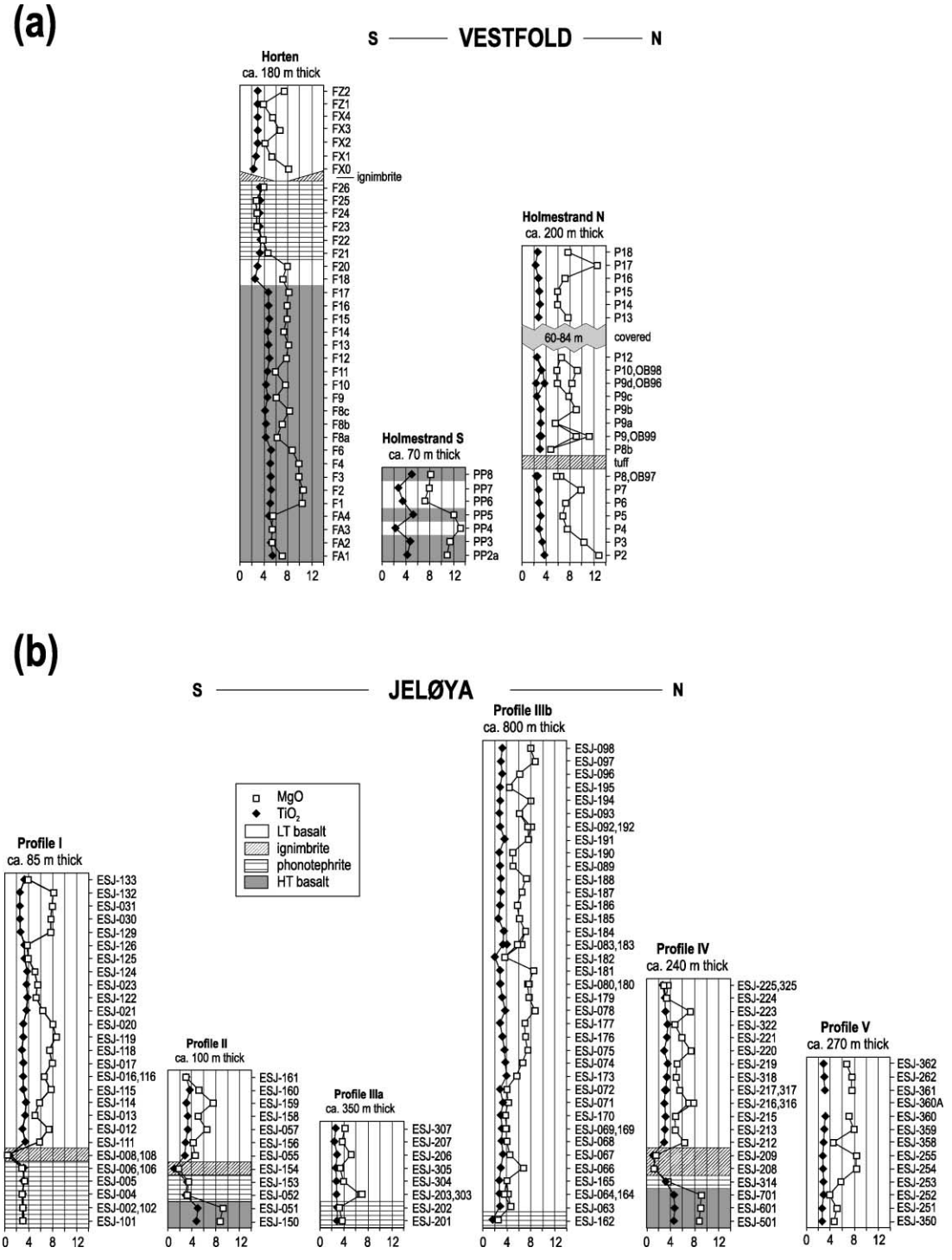

Fig. 3. Schematic presentation of the B_1 lava sequences in Vestfold (a) and Jeløya (b) discussed in this paper. The locations of the different profiles are shown in Fig. 1.

Skien area may be due to erosion as some small fault blocks in the area exhibit basalts overlain by rhomb porphyries. Magmatism was terminated with the emplacement of syenitic to granitic intrusives into the upper crust. As erosion since Permian time has removed the upper 1–2 km of the original volcanic and sedimentary sequences, cutting into shallow intrusive bodies (Fig. 1), the exposed lava sequences represent only remnants of the original lava cover. The Vestfold–Jeløya area is the only area in the Oslo rift where thick B_1 sequences are preserved in several tectonic blocks (Fig. 1), providing the possibility of obtaining information about lateral as well as time-related variations in the earliest and most primitive volcanic activity.

3. Previous work

The present work concerns the lowermost basalts in the south central part of the Oslo Graben, i.e. the Vestfold (Horten and Holmestrand) and Jeløya areas, west and east of the Oslofjord, respectively (Fig. 1). Petrographic, major and trace element data on the Horten profiles were presented by Øverli (1985) and Neumann et al. (1990); Sr–Nd–Pb isotopic data by Neumann et al. (1988, 1990). Petrographic and major element data on the Jeløya profiles are given in Schou-Jensen and Neumann (1988). These data are included in this study, where appropriate, and are used in figures and discussions. Previously unpublished major element data on the Holmestrand profiles (Toll-

Table 2
Previously unpublished trace element data for B_1 lavas in Vestfold

Profile	B1 Holmestrand S				B1 Holmestrand N					
Sample	PP2a	PP3	PP4	PP5	P7	P8	P8b	OB59	P9a	P9b
Type	HT	HT	LT	HT	LT	LT	LT	LT	LT	LT
kna*	0.40	0.44	0.43	0.44	0.44	0.44	0.33	0.35	0.37	0.41
Ba	553	524	547	325	431	293	1040	640	642	504
Rb	17	21	21	7.6	42	16	39	47	47	20
Sr	778	730	717	554	861	459	1191	799	1042	642
Cs	5.9	1.1	0.8	1.6	0.5	0.6	1.5	0.9	1.3	n.d.
Ta	5.0	5.0	4.9	5.8	3.7	2.5	2.8	4.3	3.5	3.9
Nb	77	81	79	93	61	39	44	n.d.	57	64
Hf	8.6	9.3	9.3	9.7	6.6	5.3	4.2	6.3	6.6	6.4
Zr	299	328	333	340	235	173	165	n.d.	230	233
Y	23	26	25	25	23	17	42	n.d.	29	23
Th	9.1	7.8	7.7	7.4	5.3	3.9	2.9	5.4	6.7	5.0
U	1.4	1.6	1.6	1.4	0.7	1.1	0.7	1.7	1.5	1.2
Cr	665	590	567	855	201	698	24	14	70	463
Ni	308	215	199	335	86	269	16	5	28	127
Co	60	55	53	70	40	58	35	49	45	68
Cu	111	252	230	135	117	143	15	n.d.	87	122
Pb	17	13	19	11	19	10	10	n.d.	14	9
La	63	65	63	69	50	36	81	56	47	46
Ce	144	144	144	155	105	80	190	92	101	103
Pr	18	18	17	20	13	10	25	n.d.	12	12
Nd	67	73	72	78	53	41	107	n.d.	50	48
Sm	13	14	14	15	10	7.8	21	8.0	9.4	9.4
Eu	3.3	3.7	3.5	3.8	2.8	2.1	6.2	2.7	2.5	2.5
Gd	8.3	9.5	9.6	9.6	6.6	5.7	16.0	n.d.	7.3	6.6
Tb	1.2	1.3	1.3	1.4	1.0	0.8	2.2	1.0	1.1	1.0
Dy	5.3	6.2	6.0	6.4	5.0	3.9	9.5	4.9	6.0	5.0
Ho	0.8	1.0	0.9	1.0	0.8	0.6	1.6	n.d.	1.1	0.9
Er	2.2	2.5	2.4	2.5	2.3	1.7	4.1	n.d.	2.9	2.4
Tm	0.3	0.3	0.3	0.3	n.d.	n.d.	n.d.	n.d.	n.d.	n.d.
Yb	1.4	1.7	1.6	1.5	1.9	1.2	2.9	2.4	2.7	2.0
Lu	0.2	0.2	0.2	0.2	n.d.	n.d.	n.d.	n.d.	n.d.	n.d.

Table 2 (*continued*)

Profile	B1 Holmestrand N						Younger Vestfold basalts	
Sample	P9c	P9d	P13	P14	P16	B3V1X	B3V2X	B3V3X
Type	LT	LT	LT	LT	LT	LT	LT	LT
kna *	0.49	0.39	0.56	0.40	0.43	0.30	0.47	0.52
Ba	790	769	631	760	645	438	747	556
Rb	36	56	22	52	40	55	115	107
Sr	880	868	905	957	764	634	518	393
Cs	5.2	0.5	n.d.	n.d.	n.d.	2.0	2.1	3.6
Ta	5.2	2.8	3.2	3.6	3.0	3.8	8.1	2.5
Nb	86	45	52	60	49	62	127	42
Hf	8.3	5.5	6.0	7.5	6.3	7.8	16	7.7
Zr	311	190	213	266	226	308	619	348
Y	28	23	20	29	23	42	56	42
Th	6.7	3.7	4.5	5.2	4.3	6.9	17	3.9
U	1.8	1.2	1.1	1.2	1.0	2.0	3.2	1.2
Cr	230	234	115	146	226	31	27	37
Ni	59	58	50	67	70	111	66	102
Co	52	52	47	47	51	34	16	14
Cu	206	103	88	42	86	17	16	15
Pb	12	9	13	12	12	12	11	19
La	61	46	51	45	53	103	43	
Ce	130	80	102	112	101	114	214	105
Pr	16	10	12	13	12	12.7	23.0	13.3
Nd	63	39	48	53	48	53	86	54
Sm	11	7.9	9.0	10	10	11	16	11
Eu	3.1	2.1	2.5	2.6	2.5	3.04	3.94	3.72
Gd	8.3	6.1	6.3	8.0	7.0	9.3	13	12
Tb	1.2	1.0	1.0	1.3	1.1	1.4	10.0	7.6
Ho	1.1	0.9	0.8	1.1	0.9	1.5	1.9	1.5
Er	2.9	2.4	2.1	3.1	2.5	4.2	5.4	3.6
Tm	n.d.	n.d.	n.d.	n.d.	n.d.	0.65	0.84	0.49
Yb	2.3	2.1	1.6	1.3	2.1	3.7	5.3	2.5
Lu	n.d.	n.d.	n.d.	n.d.	n.d.	0.54	0.85	0.43

Only samples for which REE have been analyzed are included. Some data on younger basaltic lavas in Vestfold are added for comparison. n.d. = Not detected, kna * = $K_2O/(K_2O + Na_2O)$. See Fig. 3 for stratigraphic positions.

efsrud, 1987), together with new trace element data on the Holmestrand and Jeløya B_1 sequences, and Sr–Nd isotope data on representative samples are presented in Tables 1–4. For comparison, the tables include data on some younger basaltic lavas from Vestfold.

4. Petrography and stratigraphy

The B_1 lavas investigated in this study are sampled along a series of profiles in the central part of the Oslo Region, west (Vestfold) and east (Jeløya) of the Oslofjord (Fig. 1). The geology, stratigraphy and petrography of these areas have been discussed by Øverli (1985), Tollefsrud (1987), Schou-Jensen and Neumann (1988), Neumann et al. (1990); here, we provide a brief summary.

The B_1 basalt sequences in Vestfold and Jeløya overlie Downtonian sandstones and are overlain by rhomb porphyry lavas (latites). The B_1 basaltic lavas in Vestfold were sampled along four profiles, two outside the town of Horten, one south of the town of Holmestrand, and one north of Holmestrand (Fig. 1). The lavas in each profile are listed in Tables 1–3 from bottom to top. The combined Horten profiles, representing the most complete stratigraphy, comprise 39 lavas with a total thickness of 180 m.

The basaltic rocks in the Jeløya area (Fig. 1) were collected along five profiles in different fault blocks. The B_1 basalt series in the different profiles are esti-

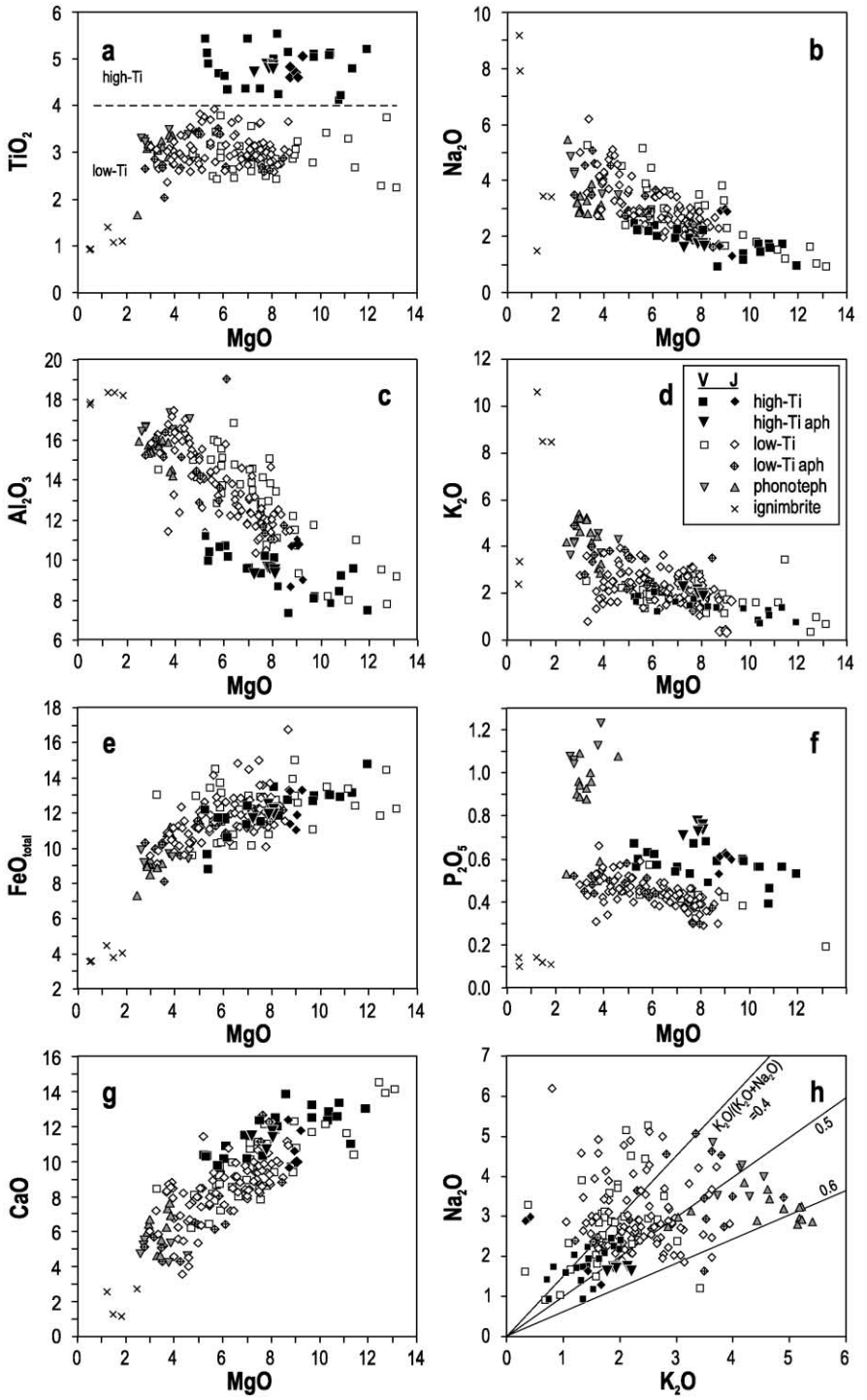

Fig. 4. Major element relations among B_1 lavas in Vestfold (V) and Jeløya (J). *Aph*: aphyric; *phonoteph*: phonotephrites.

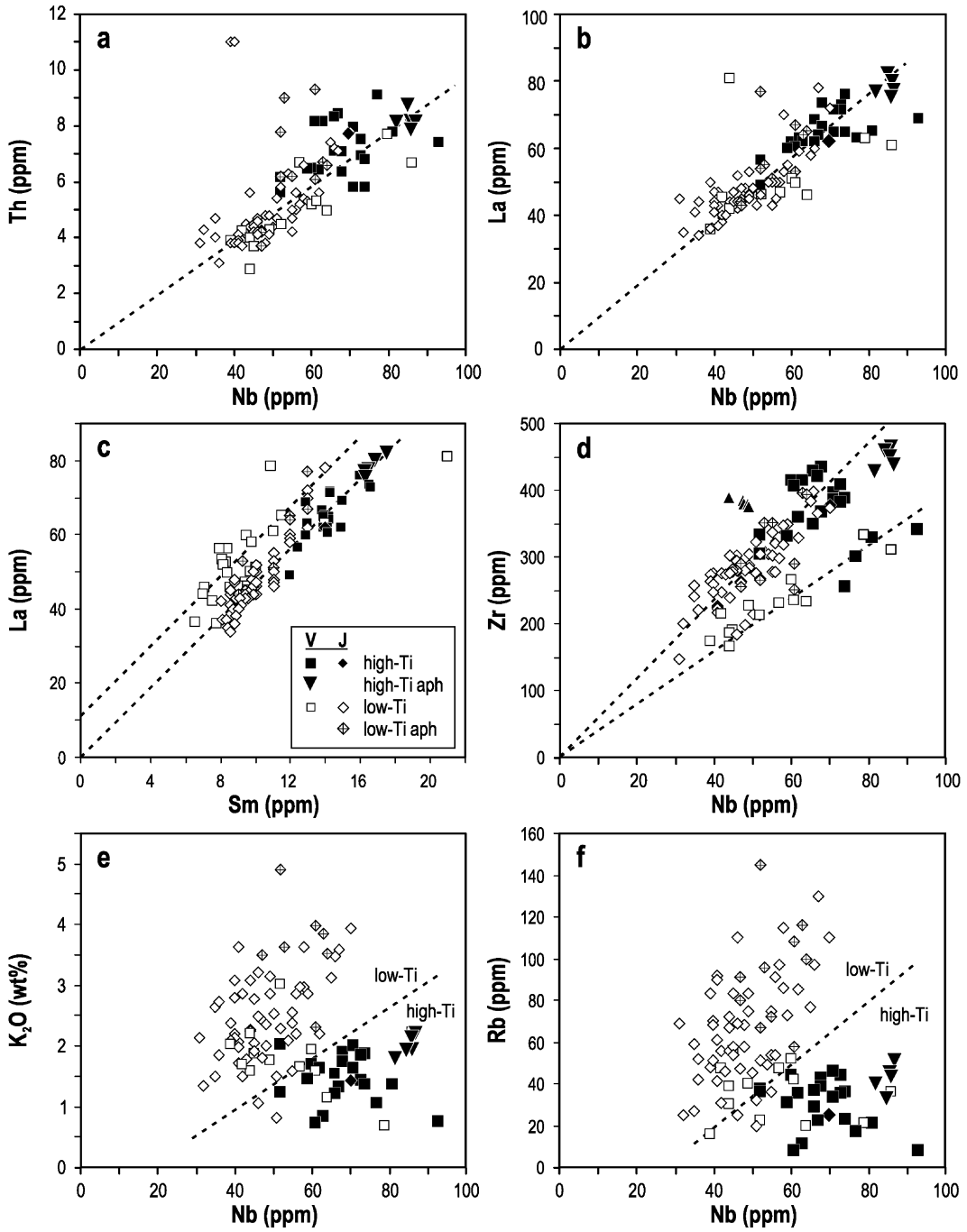

Fig. 5. Trace element relations among B_1 lavas in Vestfold (V) and Jeløya (J). *Aph*: aphyric; *phonoteph*: phonotephrites.

mated to be 100–800 m thick including some repetition within a total sequence with an estimated total thickness of 800–1500 m (Schou-Jensen and Neumann, 1988). The B_1 sequence in Jeløya east of the Oslofjord is, thus, clearly thicker than that in Vestfold to the west.

The B_1 lavas in Vestfold and Jeløya may be divided into four main groups. One group consists of high Ti (HT) ankaramites with phenocrysts of augite (cpx) and pseudomorphs after olivine (ol), with augite (near equidimensional, zoned, up to about 10 mm in diameter), as the dominant phenocryst phase. The total TiO_2 contents in the HT lavas are 4.2–5.2 wt.% (porphyritic), and 4.7–4.9 wt. % (aphyric) (Table 1). The high Ti contents are, thus, characteristic of the melts that gave rise to these lavas, not a result of high phenocryst contents. The porphyric HT lavas are classified as picrobasalts to basalts, whereas the aphyric ones fall at the basanite–basalt boundary of Le Bas et al. (1986) (Fig. 2).

Another common group is low Ti (LT) basaltic lavas containing 2.4–3.7 wt.% TiO_2. Most of the LT lavas carry phenocrysts of plagioclase (plag), augite, pseudomorphs after olivine, and titanomagnetite (mt). The LT lavas are classified as basalts to basaltic trachyandesites (Fig. 2) and, thus, tend to be somewhat more evolved than the HT lavas. Most of the LT lavas fall in the "alkaline field" (as defined by Irvine and Baragar, 1971), but some are subalkaline (Fig. 2).

The Vestfold and Jeløya B_1 sequences also include some trachybasalts to phonotephrites (Fig. 2). These have abundant tabular plagioclase phenocrysts (up to 50 mm long, generally strongly sericitized), together with scattered phenocrysts of titanomagnetite, and microphenocrysts of augite, plagioclase, apatite (ap) and altered olivine. Finally, the profiles exhibit a few ignimbrites and tuffs of trachytic composition.

The largest sequence of HT basalts (21 flows) is exhibited at the base of the combined Horten profiles in Vestfold, where the five youngest HT lavas are aphyric (F13–F17; Fig. 3). The HT basalts are overlain by two LT basalts, followed by a series of phonotephrites. The phonotephrites are locally overlain by an ignimbrite that looks very similar to those found in Jeløya, and the uppermost part of the Horten profile consists of LT lavas. HT lavas are also found in the Holmestrand S profile in Vestfold, where they alternate with LT lavas.

The Jeløya Profiles II and IV show a sequence very similar to the Horten profile with HT lavas at the base, overlain by phonotephrites and followed by ignimbrites, while the upper part of the sequences consists of LT lavas (Fig. 3). In contrast to the many HT lavas at the base of the Horten profile, the Jeløya Profiles II and IV exhibit only two and three HT flows, respectively. However, the Jeløya HT sequence continues below sea level and is clearly thicker than the sequence sampled. The Jeløya Profile I shows a similar stratigraphy to II and IV, but HT basalts are missing. In the Jeløya Profiles IIIa, IIIb, and V and in the Holmestrand N profile, only LT basalts have been observed, with the exception of a tuff below lava P8b in the Holmestrand N profile (Fig. 3).

Both the HT and the LT lavas show significant stratigraphic variations with respect to MgO contents and other parameters reflecting the degree of fractionation. These variations include local, gradual upwards decreases in MgO, interrupted by abrupt increases in MgO (e.g. the lower part of the Horten and Holmestrand profiles and the middle part of Jeløya Profile I; Fig. 3), and local, gradual upwards increases in MgO, (e.g. the middle part of Jeløya Profile IIIb).

5. Compositional relations

5.1. Analytical methods

Major elements were analyzed on fused pellets using 9:1 dilution with sodium tetraborate, and mass absorption corrections. The analyses were performed on a Philips PW 2400 X-ray fluorescence spectro-

Fig. 6. Primordial mantle-normalized trace element patterns (normalization factors, PM, from McDonough and Sun, 1995) for representative B_1 basaltic lavas and associated evolved rocks in Vestfold and Jeløya. The different basalt groups are divided into "least altered", ($0.45 \leq K_2O/(K_2O+Na_2O) \leq 0.6$) and "most altered" ($K_2O/(K_2O+Na_2O)$ ratios < 0.45 or >0.6). For each basalt group the total range is shown in gray; for the phonotephrites the Vestfold range is shown in gray and the Jeløya range in diagonal stripes. *V*: Vestfold; *J*: Jeløya. Notice that the phonotephrite–ignimbrite diagram has a different scale. See text for discussion.

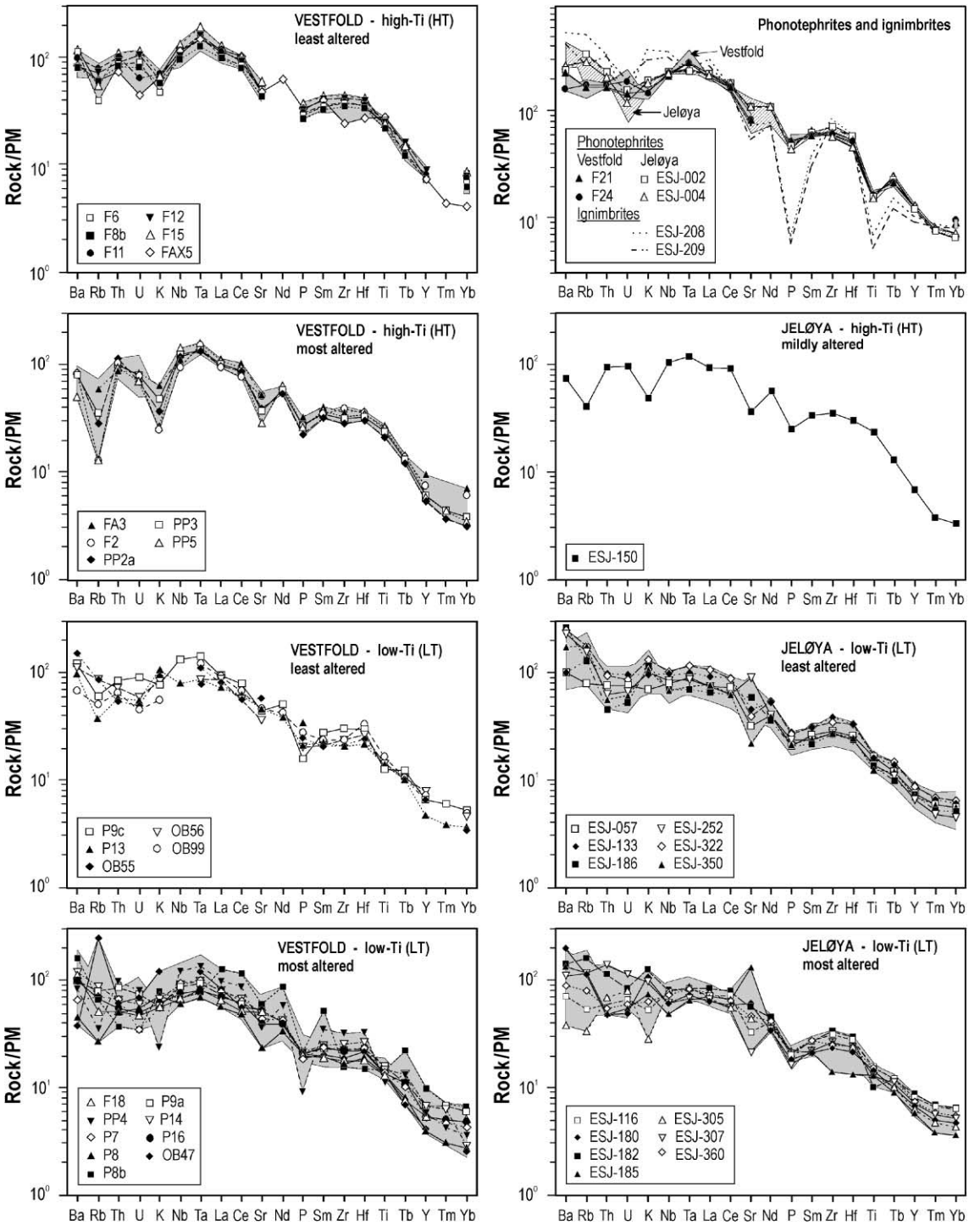
VESTFOLD - high-Ti (HT)
least altered
F6
F8b
F11
F12
F15
FAX5
Phonotephrites and ignimbrites
Vestfold
Jeløya
Phonotephrites
Vestfold
Jeløya
F21
F24
ESJ-002
ESJ-004
Ignimbrites
ESJ-208
ESJ-209
VESTFOLD - high-Ti (HT)
most altered
FA3
F2
PP2a
PP3
PP5
JELØYA - high-Ti (HT)
mildly altered
ESJ-150
VESTFOLD - low-Ti (LT)
least altered
P9c
P13
OB55
OB56
OB99
JELØYA - low-Ti (LT)
least altered
ESJ-057
ESJ-133
ESJ-186
ESJ-252
ESJ-322
ESJ-350
VESTFOLD - low-Ti (LT)
most altered
F18
PP4
P7
P8
P8b
P9a
P14
P16
OB47
JELØYA - low-Ti (LT)
most altered
ESJ-116
ESJ-180
ESJ-182
ESJ-185
ESJ-305
ESJ-307
ESJ-360
Rock/PM
Ba Rb Th U K Nb Ta La Ce Sr Nd P Sm Zr Hf Ti Tb Y Tm Yb

graph with X47 software at the Institute of Geology, University of Oslo. Trace element concentrations were determined by two methods. All bulk rock samples were analyzed for selected trace elements by X-ray fluorescence (XRF) spectrometry on pressed powder pellets (Table 2).

A number of representative samples were also analyzed for trace elements by Inductively Coupled Plasma Mass Spectrometry (ICP-MS) at ACTLABS (Ancaster, Ontario, Canada). Analytical precision is given in Neumann et al. (1990) and Dunworth and Bell (2001), respectively. Comparisons of the two datasets show some discrepancies, in particular, the more recent ICP-MS data show lower HREE concentrations. This will be discussed in a later section.

Sr and Nd isotope analyses were carried out on unleached whole-rock powders from Jeløya; whole-rock element concentrations, as measured by ICP-MS, were used to age-correct the measured data. Pyroxene separates [500–250 μm diameter] were hand picked in ethanol, taking care to avoid grains with visible cracks and inclusions. They were subsequently washed in ethanol and water and leached in 6 N HCl at 100 °C for 4 h, before being dried, weighed, and dissolved. Dissolution was carried out in sealed 15 ml Savillex beakers using $HNO_3–HF–HClO_4$ mixtures held at 120 °C for 48 h. Subsequent chemical and mass spectrometric procedures were based on those described by Mearns (1986) and Neumann et al. (1990).

Sm–Nd element concentrations were measured by isotope dilution; test runs of Rb–Sr isotope dilution measurements were not reproducible, believed to be due to Rb-bearing melt inclusion and alteration products not sufficiently removed by whole-grain acid leaching. Laser-ICPMS data from these samples (unpublished) suggest that the true Rb/Sr ratios of the pyroxenes are both consistent and <0.005 and, thus, measured $^{87}Sr/^{86}Sr$ values only are given in Table 4.

Mass spectrometry was carried out in three locations during a 28-month period: (i) Sr from whole-rock samples and Rb from pyroxenes were analyzed on a VG 354 mass spectrometer and Sm–Nd from whole-rock and pyroxene separate samples were analyzed on a Finnegan-MAT 262 mass spectrometer at the Mineralogisk-Geologisk Museum, University of Oslo; (ii) Pyroxene separates were analyzed for Sr on a Finnegan-MAT 261 and Sm–Nd–Sr on a Finnegan-MAT 262 at the Vrije Universiteit in Amsterdam; and (iii) Sr and Nd pyroxene separate analyses were carried out on a Finnegan-MAT 261 at Carleton Unversity, Ottawa. All Sr and Nd isotopic compositions were corrected for within-run mass fractionation by normalizing to $^{86}Sr/^{88}Sr = 0.1194$ and $^{146}Nd/^{144}Nd = 0.7219$, respectively. Dataset cross-calibration to ensure reproducibility between different datasets involved repeated measurements of the NBS 987 (Sr) and the La Jolla and SCS A Nd standards with associated sample results corrected, according to internationally accepted values (0.71025, 0.51186, and 0.51111, respectively), as well as analysis of a small subset of samples on different machines at different times.

5.2. Major element chemistry

The lavas in the B_1 sequence in Vestfold range in MgO contents from 2.6 to 13.2 wt.%, and in Jeløya from 0.5 to 9.1 wt.%, with a range of 8.1–7.3 wt.% among aphyric lavas in Vestfold and 8.5–2.9 in Jeløya (Fig. 4). The HT basalts generally have higher MgO than the LT basalts although the highest MgO contents occur in some of the LT basalts. On the average, the B_1 lavas in Vestfold are somewhat more mafic than those in Jeløya (Fig. 4), and the HT basalts are more mafic than the LT basalts. Typically, CaO and FeO_{total} decrease, and Al_2O_3, Na_2O, K_2O, and P_2O_5 increase with decreasing MgO (Fig. 4) although the different oxides show considerable scatter. This is particularly true for K_2O, which occurs in very low concentrations in some samples. The scatter in K_2O is reflected in a wide range in values of the $K_2O/(K_2O + Na_2O)$ ratio (0.1 to 0.8) although the majority of the samples fall in the range 0.4–0.6 (Fig. 4). In addition to higher TiO_2 contents, the HT series (TiO_2>4 wt.%) has higher P_2O_5 and, generally, lower Al_2O_3, K_2O and Na_2O contents than LT lavas ($TiO_2 < 4$ wt.%) with similar MgO concentrations (Fig. 4).

5.3. Trace element chemistry

The lavas show moderate scatter in the ratios between the most highly incompatible trace elements which are not easily mobilized during alteration, e.g. Th/Nb and La/Nb (Fig. 5a, b), whereas in La–Sm and Zr–Nb plots, HT basalts from Vestfold and Jeløya

Table 3
Previously unpublished trace element data for B_1 lavas in Jeløya

Profile	I								II	
Sample	ESJ-002	ESJ-004	ESJ-006	ESJ-116	ESJ-017	ESJ-118	ESJ-021	ESJ-133	ESJ-150	ESJ-057
Type	phon	phon	phon	LT	LT	LT	LT	LT-aph	HT	LT
kna *	0.65	0.62	0.64	0.33	0.34	0.37	0.54	0.51	0.47	0.49
Ba	1540	1720	1710	460	377	387	1020	677	498	684
Rb	196	169	158	32	27	31	77	82	25	49
Sr	2100	2150	2560	648	521	509	860	932	738	643
Cs	3.4	1.4	1.8	0.9	n.d.	n.d.	n.d.	1.1	0.5	n.d.
Ga	31	31	31	22	14	18	26	25	18	19
Ta	8.5	8.9	8.5	3.1	2.7	2.7	3.9	3.8	4.5	3.5
Nb	148	144	146	51	35	42	65	67	70	54
Hf	16	13	15	7.8	6.3	5.9	9.1	10	8.7	7.4
Zr	737	591	718	322	257	246	383	412	377	305
Y	52	56	54	35	31	30	35	40	30	33
Th	18	16	15	4.7	4.0	3.9	7.4	8.1	7.7	6.3
U	3.1	2.4	1.9	1.3	1.1	1.1	1.6	2.0	2.0	1.6
Cr	n.d.	n.d.	n.d.	227	240	259	124	11	534	119
Ni	24	13	15	99	55	100	66	57	169	43
Co	33	26	29	59	27	46	49	45	44	37
V	190	205	195	345	267	309	351	272	379	327
Cu	215	180	369	92	27	49	70	101	64	51
Pb	16	6	10	n.d.	n.d.	n.d.	10	17	n.d.	n.d.
Zn	165	88	134	69	n.d.	65	134	120	20	n.d.
Sn	4	4	4	2	n.d.	2	2	3	2	n.d.
W	59	53	52	55	40	96	39	64	75	29
Mo	2.3	1.6	1.7	2.3	0.6	0.8	1.8	1.5	1.1	n.d.
La	139	138	121	46	n.d.	38	58	62	62	50
Ce	297	298	280	118	102	98	148	157	158	127
Pr	37.1	36.9	35.3	12.8	11.2	10.8	16.1	18.4	19.1	13.8
Nd	134	135	130	50	43	41	59	68	72	52
Sm	25	26	25	11	9.2	8.9	12.0	13.0	14.0	11.0
Eu	6.61	6.98	6.68	2.73	2.43	2.37	3.16	3.62	4.04	2.73
Gd	18	19	18	8.3	7.1	6.9	8.9	10	11	8.0
Tb	2.2	2.4	2.3	1.2	1.1	1.1	1.3	1.4	1.3	1.2
Dy	11	12	11	6.6	5.7	5.6	8.9	7.3	6.3	6.3
Ho	1.8	1.9	1.8	1.2	1.0	1.0	1.2	1.3	1.0	1.2
Er	4.5	4.9	4.5	3.1	2.8	2.7	3.2	3.5	2.5	3.0
Tm	0.51	0.55	0.52	0.45	0.38	0.38	0.43	0.46	0.26	0.41
Yb	2.9	3.2	3.1	2.8	2.4	2.3	2.7	2.7	1.5	2.5
Lu	0.43	0.48	0.45	0.42	0.37	0.36	0.41	0.44	0.23	0.39

(continued on next page)

Table 3 (*continued*)

Profile	II			IIIa						
Sample	ESJ-158	ESJ-159	ESJ-160	ESJ-201	ESJ-202	ESJ-203	ESJ-303	ESJ-304	ESJ-305	ESJ-206
Type	LT	LT	LT	phon	phon	LT	LT	LT	LT	LT
kna *	0.47	0.53	0.58	0.60	0.38	0.49	0.53	0.36	0.12	0.42
Ba	534	746	793	1600	746	1500	1470	679	246	613
Rb	51	59	97	154	67	52	72	67	20	68
Sr	645	586	787	1520	531	810	1450	621	845	527
Cs	1.4	n.d.	1.0	475	1.0	n.d.	n.d.	1.1	n.d.	1.1
Ga	18	13	26	23	18	12	18	18	18	22
Ta	3.1	2.7	3.9	3.3	3.4	2.5	2.7	2.7	3.1	2.9
Nb	52	35	66	55	52	36	44	44	51	48
Hf	7.4	6.0	10	7.3	6.4	5.4	6.5	7.3	6.7	6.9
Zr	305	240	398	309	265	220	276	302	276	280
Y	33	27	37	33	33	26	27	35	27	33
Th	5.8	4.7	7.2	5.8	6.2	n.d.	4.4	5.6	5.4	4.8
U	1.7	1.2	1.7	1.6	1.9	0.9	1.0	1.6	1.6	1.2
Cr	105	212	55	15	210	105	104	26	n.d.	104
Ni	52	129	72	n.d.	n.d.	n.d.	77	39	39	65
Co	34	32	48	49	26	28	54	25	33	48
V	306	301	359	267	226	278	305	313	207	375
Cu	121	152	83	n.d.	n.d.	n.d.	34	n.d.	97	56
Pb	n.d.	n.d.	14	11	n.d.	n.d.	18	n.d.	9	6
Zn	45	n.d.	124	103	13	n.d.	108	32	60	58
Sn	1	n.d.	2	2	1	n.d.	7	1	2	2
W	41	27	41	86	42	32	60	14	30	13
Mo	n.d.	n.d.	1.4	1.5	0.5	n.d.	0.8	n.d.	0.7	0.6
La	46	41	60	57	54	44	44	44	43	48
Ce	119	102	150	118	113	95	95	99	92	102
Pr	14.1	12.2	17.9	14.2	13.8	11.7	11.8	12.4	11.5	12.5
Nd	52	45	65	55	52	45	46	49	45	49
Sm	10	8.7	12	11	10	8.8	8.6	10	8.9	11
Eu	2.80	2.49	3.48	2.89	2.80	2.39	2.36	2.71	2.55	2.79
Gd	8.1	6.9	9.6	8.4	8.3	6.9	7.2	8.6	7.4	8.6
Tb	1.1	0.9	1.3	1.2	1.2	1.0	1.0	1.2	1.0	1.2
Dy	5.9	4.9	6.9	6.1	6.1	4.9	5.0	6.4	5.1	6.4
Ho	1.1	0.9	1.3	1.1	1.1	0.9	0.9	1.2	0.9	1.1
Er	2.9	2.3	3.3	3.1	3.1	2.5	2.5	3.3	2.5	3.1
Tm	0.38	0.30	0.44	0.40	0.42	0.32	0.32	0.45	0.32	0.41
Yb	2.3	1.8	2.6	2.5	2.6	1.9	2.0	2.7	1.9	2.6
Lu	0.37	0.29	0.43	0.39	0.40	0.30	0.32	0.43	0.30	0.39

Profile	IIIa			IIIb						
Sample	ESJ-207	ESJ-307	ESJ-176	ESJ-078	ESJ-179	ESJ-080	ESJ-180	ESJ-181	ESJ-182	ESJ-083
Type	LT	LT	LT	LT	LT	LT	LT	LT-aph	LT-aph	LT
kna *	0.43	0.43	0.56	0.52	0.63	0.46	0.60	0.68	0.44	0.65
Ba	571	719	747	724	1200	862	1300	1090	939	1130
Rb	83	70	56	42	83	56	68	91	96	115
Sr	401	419	598	713	1280	1030	1220	869	1120	1400
Cs	1.5	1.1	n.d.	0.5	1.3	n.d.	0.9	1.1	1.7	1.4
Ga	20	19	15	18	22	17	16	18	26	25
Ta	2.4	2.5	2.6	2.4	3.0	3.0	2.7	2.9	3.1	3.5
Nb	39	40	42	36	49	44	40	47	53	58
Hf	6.5	6.8	6.7	5.9	7.4	5.9	6.1	6.8	8.4	7.7
Zr	263	275	275	221	304	238	247	256	351	319
Y	31	31	30	26	32	29	29	29	38	33
Th	11.0	11.0	3.7	3.1	4.1	4.4	3.8	4.2	9.0	5.4
U	2.3	2.3	1.0	0.8	1.0	0.9	1.0	1.0	1.7	1.1
Cr	17	18	113	235	153	148	157	205	n.d.	82
Ni	39	63	45	141	142	83	65	98	16	69
Co	52	49	27	93	69	61	41	62	30	56
V	296	275	352	537	348	320	302	310	157	336
Cu	75	17	67	193	354	25	40	179	30	122
Pb	16	13	n.d.	n.d.	8	n.d.	n.d.	12	8	8
Zn	126	96	n.d.	115	146	43	28	111	83	137
Sn	2	2	n.d.	3	2	2	1	2	2	2
W	63	56	17	101	59	109	67	76	83	48
Mo	1.0	0.5	n.d.	0.6	1.1	0.5	n.d.	0.9	1.2	0.6
La	50	43	40	34	45	44	41	43	55	53
Ce	102	93	101	87	111	108	99	106	132	132
Pr	12.4	11.4	12.3	9.9	13.4	11.9	11.9	12.6	15.6	14.2
Nd	48	44	46	39	50	45	43	46	57	54
Sm	10	8.9	9.0	8.6	9.8	9.3	8.6	9.1	11	11
Eu	2.83	2.27	2.63	2.32	2.89	2.52	2.56	2.69	3.02	3.02
Gd	8.4	7.7	7.6	6.7	8.2	7.1	7.2	7.6	8.8	8.5
Tb	1.2	1.1	1.0	1.0	1.1	1.0	1.0	1.1	1.2	1.3
Dy	5.9	5.6	5.5	5.1	5.8	n.d.	5.3	5.7	6.6	6.4
Ho	1.0	1.0	1.0	0.9	1.0	1.0	1.0	1.0	1.2	1.1
Er	2.9	2.9	2.6	2.3	2.7	2.6	2.5	2.8	3.4	3.0
Tm	0.38	0.39	0.34	0.30	0.36	0.36	0.34	0.37	0.47	0.39
Yb	2.3	2.3	2.1	1.9	2.1	2.2	2.1	2.3	2.9	2.4
Lu	0.36	0.38	0.33	0.28	0.34	0.34	0.34	0.36	0.47	0.37

(continued on next page)

Table 3 (*continued*)

Profile	IIIb									
Sample	ESJ-184	ESJ-185	ESJ-186	ESJ-187	ESJ-188	ESJ-190	ESJ-191	ESJ-092	ESJ-093	ESJ-194
Type	LT	LT	LT-aph	24	LT	LT	LT	LT	LT-aph	LT
kna *	0.49	0.39	0.50	0.40	0.35	0.50	0.51	0.49	0.39	0.27
Ba	1620	856	1800	1100	947	1150	1100	1160	1280	979
Rb	47	69	80	54	36	61	54	58	58	25
Sr	882	2590	1220	1490	1660	972	827	955	1390	1210
Cs	n.d.	2.3	1.3	0.8	2.0	2.6	3.9	4.3	8.5	11.0
Ga	18	21	21	18	27	16	26	19	23	17
Ta	2.9	2.4	2.7	3.2	3.2	2.9	3.3	3.1	3.7	3.0
Nb	47	31	47	55	55	41	56	48	61	46
Hf	6.4	3.7	6.9	7.3	6.8	5.7	7.0	5.4	6.0	4.6
Zr	263	146	289	302	277	217	277	197	252	184
Y	29	25	32	33	33	28	30	29	27	23
Th	4.3	3.8	3.7	4.7	4.2	3.8	5.0	3.8	6.1	4.1
U	1.0	1.1	1.1	1.3	1.0	0.8	1.3	0.6	1.7	1.1
Cr	199	82	88	114	73	28	93	262	68	144
Ni	80	72	98	78	57	n.d.	n.d.	120	62	n.d.
Co	45	53	51	60	47	26	66	61	49	38
V	287	292	313	246	389	240	474	331	268	280
Cu	21	29	73	30	217	n.d.	n.d.	145	82	n.d.
Pb	n.d.	n.d.	16	6	6	n.d.	9	5	12	n.d.
Zn	70	35	110	83	92	16	123	45	99	38
Sn	1	1	2	2	2	n.d.	2	2	3	1
W	86	33	46	90	32	37	80	65	65	51
Mo	n.d.	0.7	0.6	0.7	0.6	n.d.	0.8	n.d.	0.9	n.d.
La	45	45	44	50	43	47	45	48	53	42
Ce	112	109	108	122	108	111	113	118	127	89
Pr	13.3	12.8	12.6	14.6	13.0	13.2	13.5	12.9	13.2	10.6
Nd	49	46	46	54	48	48	50	49	48	41
Sm	9.4	8.6	9.0	10	9.4	8.8	9.7	9.8	9.3	8.0
Eu	2.78	2.70	2.63	3.08	2.88	2.68	2.90	2.69	2.64	2.30
Gd	7.8	6.8	7.5	8.3	7.9	7.2	8.0	7.3	6.9	6.3
Tb	1.0	0.9	1.0	1.1	1.1	1.0	1.1	1.1	1.0	0.9
Dy	5.4	4.6	5.5	6.0	5.9	5.1	5.6	5.6	5.1	4.4
Ho	1.0	0.8	1.0	1.1	1.1	0.9	1.0	1.0	0.9	0.8
Er	2.6	2.1	2.7	2.8	3.1	2.6	2.7	2.6	2.4	2.2
Tm	0.34	0.26	0.36	0.37	0.40	0.33	0.33	0.34	0.32	0.27
Yb	2.0	1.6	2.3	2.2	2.5	1.9	1.9	2.1	2.0	1.7
Lu	0.33	0.26	0.36	0.36	0.41	0.32	0.31	0.33	0.32	0.27

Profile	IIIb			IV						
Sample	ESJ-195	ESJ-096	ESJ-098	ESJ-314	ESJ-208	ESJ-209	ESJ-212	ESJ-213	ESJ-215	ESJ-216
Type	LT	LT	LT	phon	ign	ign	LT	LT	LT	LT
kna *	0.33	0.33	0.34	0.52	0.88	0.71	0.28	0.47	0.47	0.52
Ba	592	663	553	2770	3470	2720	374	1120	879	481
Rb	45	41	33	94	300	159	25	91	73	58
Sr	709	948	638	1220	1450	1050	1230	1910	1090	622
Cs	2.5	184	1.6	1.1	1.8	0.9	n.d.	0.7	0.6	n.d.
Ga	18	15	22	31	30	24	14	24	27	21
Ta	3.3	3.2	n.d.	8.2	8.8	8.1	2.2	3.3	3.5	2.9
Nb	50	41	n.d.	143	231	205	32	56	59	45
Hf	5.2	5.5	n.d.	16	17	16	5.1	7.8	8.4	7.0
Zr	214	225	n.d.	706	878	778	200	321	349	280
Y	n.d.	26	n.d.	52	45	40	26	32	37	32
Th	4.4	4.1	n.d.	16	26	25	4.3	5.6	5.3	4.5
U	1.6	1.3	n.d.	1.6	2.5	3.9	0.9	1.2	1.4	1.2
Cr	n.d.	39	254	n.d.	n.d.	34	48	22	109	316
Ni	n.d.	21	95	38	n.d.	17	28	32	58	126
Co	26	32	69	26	12	12	42	51	44	54
V	224	286	399	182	199	113	313	302	310	318
Cu	n.d.	22	78	134	n.d.	15	39	607	93	88
Pb	n.d.	n.d.	9	17	17	8	n.d.	8	5	7
Zn	35	n.d.	116	152	115	94	10	120	103	71
Sn	1	n.d.	2	4	1	2	n.d.	2	2	2
W	30	64	71	24	52	41	64	28	36	54
Mo	n.d.	n.d.	1.0	1.3	1.1	0.7	n.d.	0.9	1.1	1.0
La	48	43	41	128	188	168	35	50	55	43
Ce	100	108	103	246	280	273	80	111	118	94
Pr	11.8	11.7	11.4	33.4	31.7	30.2	10.0	13.6	14.4	11.7
Nd	45	44	44	125	97	90	41	53	56	46
Sm	8.8	9.1	9.2	23	15	12	8.4	11	11	9.6
Eu	2.53	2.58	2.53	6.34	3.87	3.20	2.32	2.94	3.07	2.60
Gd	6.9	6.8	7.2	18	11	8.9	n.d.	8.5	9.0	8.0
Tb	1.0	1.0	1.0	2.2	1.5	1.2	0.9	1.20	1.30	1.10
Dy	4.9	5.2	5.4	10.0	7.7	6.8	5.0	6.00	6.90	6.20
Ho	0.9	0.9	1.0	1.7	1.5	1.3	0.9	1.1	1.3	1.1
Er	2.5	2.4	2.5	4.7	4.3	4.0	2.4	3.0	3.5	3.1
Tm	0.34	0.30	0.33	0.51	0.60	0.57	0.32	0.39	0.47	0.41
Yb	2.1	1.9	2.0	3.0	3.6	3.5	1.9	2.4	2.9	2.5
Lu	0.32	0.29	0.31	0.44	0.57	0.56	0.29	0.37	0.45	0.39

(continued on next page)

Table 3 (*continued*)

Profile	IV									
Sample	ESJ-316	ESJ-217	ESJ-317	ESJ-318	ESJ-219	ESJ-220	ESJ-221	ESJ-322	ESJ-223	ESJ-224
Type	LT	LT	LT	LT-aph	LT-aph	LT	LT-aph	LT	LT	LT
kna *	0.44	0.46	0.50	0.59	0.55	0.48	0.49	0.58	0.59	0.50
Ba	469	658	679	869	1230	475	762	1710	855	689
Rb	46	75	75	116	100	54	72	110	86	130
Sr	564	835	779	1290	1100	627	781	812	611	1640
Cs	n.d.	0.5	n.d.	0.7	n.d.	n.d.	n.d.	1.5	n.d.	0.7
Ga	18	24	19	25	23	20	n.d.	25	27	26
Ta	2.8	3.4	3.2	3.9	3.8	2.8	3.2	4.5	3.4	3.9
Nb	43	55	49	63	64	45	55	70	58	67
Hf	6.7	8.0	6.9	10	10	6.8	8.3	10	8.4	8.6
Zr	274	337	284	396	394	278	352	374	346	366
Y	31	37	34	40	40	31	37	38	34	34
Th	4.5	5.0	4.8	6.7	6.6	4.4	6.2	7.8	6.6	7.1
U	1.2	1.3	1.3	1.6	1.6	1.2	1.3	1.8	1.4	1.6
Cr	247	151	128	51	57	305	71	n.d.	195	15
Ni	112	100	65	68	95	115	42	43	137	96
Co	45	50	29	45	44	53	51	24	46	33
V	274	314	257	359	329	319	380	288	332	246
Cu	80	103	56	81	98	81	65	52	88	72
Pb	n.d.	6	n.d.	12	13	5	8	n.d.	12	1
Zn	46	89	26	132	145	58	98	26	123	97
Sn	2	2	1	2	2	2	2	2	2	2
W	69	57	44	25	20	57	39	23	12	21
Mo	1.0	0.9	n.d.	1.1	1.1	1.2	1.1	0.7	1.7	1.0
La	40	n.d.	46	64	65	44	51	72	70	78
Ce	85	113	102	135	137	93	114	153	145	162
Pr	10.9	13.9	12.6	16.1	16.6	11.5	14.0	17.7	17.2	18.9
Nd	43	54	49	62	64	46	55	69	65	71
Sm	8.7	11	9.9	12	12	9.4	11	13	13	14
Eu	2.43	2.96	2.72	3.28	3.27	2.57	2.89	3.55	3.28	3.68
Gd	7.6	8.9	8.5	10	10	7.5	8.8	11	9.8	10
Tb	1.10	1.30	1.20	1.50	1.40	1.1	1.3	1.5	1.4	1.4
Dy	5.60	6.70	6.20	7.50	7.50	5.9	6.6	7.3	6.9	6.9
Ho	1.0	1.2	1.2	1.4	1.4	n.d.	1.2	1.3	1.2	1.2
Er	2.9	3.5	3.3	4.0	3.9	3.0	3.4	3.7	3.5	3.5
Tm	0.38	0.46	0.44	0.5	0.53	0.40	0.46	0.48	0.45	0.44
Yb	2.4	2.9	2.7	3.4	3.2	2.5	2.9	2.9	2.7	2.7
Lu	0.37	0.44	0.43	0.53	0.50	0.38	0.44	0.45	0.42	0.40

Profile	IV		V							
Sample	ESJ-225	ESJ-325	ESJ-350	ESJ-251	ESJ-252	ESJ-353	ESJ-254	ESJ-255	ESJ-358	ESJ-359
Type	LT-aph	LT-aph	LT	LT	LT	LT	LT	LT	LT	LT
kna *	0.58	0.53	0.46	0.37	0.50		0.47	0.44	0.31	0.57
Ba	1260	1310	1190	723	1580	952	899	903	821	740
Rb	145	108	110	69	97	73	92	90	85	83
Sr	1190	1040	450	1820	1840	935	889	841	1360	725
Cs	0.6	0.6	1.2	2.6	3.5	5.2	1.4	3.8	1.9	1.1
Ga	18	24	22	20	22	21	17	17	22	23
Ta	3.4	3.8	2.8	2.8	3.3	3.0	2.5	2.5	3.9	2.8
Nb	52	61	46	46	57	49	41	41	62	45
Hf	n.d.	10	7.2	7.0	6.8	7.2	5.4	5.5	8.2	7.2
Zr	267	289	293	302	297	288	223	226	329	282
Y	38	41	31	31	29	30	24	24	32	30
Th	7.8	9.3	4.6	4.7	5.2	4.8	3.8	3.9	5.6	4.2
U	2.1	2.4	1.3	1.3	1.4	1.3	1.0	1.0	1.5	1.1
Cr	n.d.	n.d.	70	57	14	98	196	200	n.d.	194
Ni	52	18	41	55	n.d.	87	113	106	39	107
Co	29	34	32	37	38	51	62	54	41	62
V	162	185	226	235	245	336	321	316	238	398
Cu	34	26	19	28	n.d.	143	53	53	82	91
Pb	n.d.	9	10	6	13	9	n.d.	6	n.d.	6
Zn	36	109	87	77	138	104	73	72	68	89
Sn	1	2	1	1	2	2	1	1	2	2
W	38	24	29	39	46	63	68	50	44	34
Mo	0.6	0.7		0.9	1.0	1.7	0.5	0.6	1.6	1.1
La	77	67	52	44	50	53	37	37	59	47
Ce	155	140	109	96	109	113	80	82	125	101
Pr	18.1	16.3	13.0	12.2	13.5	13.3	10.2	10.4	15.0	12.2
Nd	68	64	51	48	52	53	40	41	59	49
Sm	13	13	10	9.3	9.9	11	8.1	8.3	12	10
Eu	3.28	3.30	n.d.	2.63	2.91	2.93	2.30	2.37	3.37	2.78
Gd	10	11	8.3	7.9	8.1	8.5	6.8	6.9	9.3	8.3
Tb	1.5	1.5	1.2	1.1	1.1	1.2	0.9	0.9	1.3	1.2
Dy	7.4	7.8	6.0	5.6	5.4	5.9	4.6	4.6	6.4	5.9
Ho	1.4	1.5	1.1	1.0	1.0	1.10.8	0.8	1.1	1.1	
Er	3.9	4.1	3.1	2.9	2.7	2.9	2.2	2.2	3.0	2.9
Tm	0.51	0.54	0.41	0.38	0.33	0.38	0.28	0.27	0.38	0.38
Yb	3.1	3.4	2.5	2.3	2.0	2.3	1.6	1.7	2.3	2.3
Lu	0.48	0.53	0.39	0.37	0.32	0.35	0.26	0.26	0.35	0.35

(continued on next page)

Table 3 (*continued*)

Profile	V				
Sample	ESJ-360	ESJ-360A	ESJ-361	ESJ-262	ESJ-362
Type	LT	LT	LT	LT	LT
kna*	0.37	0.41	0.46	0.47	
Ba	583	908	656	671	628
Rb	47	81	68	48	51
Sr	910	899	842	663	725
Cs	0.7	1.2	1.0	0.9	1.2
Ga	19	21	22	19	23
Ta	3.0	2.9	2.6	2.4	2.6
Nb	47	46	40	39	40
Hf	6.8	7.1	6.6	6.6	6.6
Zr	261	279	260	274	260
Y	32	30	32	31	32
Th	4.3	4.2	3.8	3.8	3.8
U	1.2	1.1	0.9	0.9	0.9
Cr	163	164	165	114	108
Ni	89	102	108	121	83
Co	48	65	67	44	53
V	361	367	365	277	341
Cu	241	45	43	213	119
Pb	n.d.	12	7	5	6
Zn	64	122	105	48	77
Sn	1	2	2	1	2
W	42	65	58	30	56
Mo	0.8	1.2	1.2	0.8	0.6
La	48	44	47	36	44
Ce	106	100	106	84	96
Pr	12.7	12.1	13.0	10.7	11.7
Nd	51	49	52	42	47
Sm	11	9.9	11	8.8	9.9
Eu	2.74	2.73	2.88	2.42	2.67
Gd	8.7	8.3	8.8	7.6	8.2
Tb	1.2	1.2	1.3	1.1	1.2
Dy	6.2	5.8	6.3	5.6	6.2
Ho	1.1	1.0	1.1	1.0	1.1
Er	3.1	2.9	3.2	2.9	3.1
Tm	0.40	0.37	0.41	0.38	0.42
Yb	2.4	2.3	2.5	2.4	2.7
Lu	0.37	0.35	0.38	0.38	0.41

Sample numbering follows that of Schou-Jensen and Neumann (1988). Only samples for which REE have been analyzed are included. n.d. = Not detected, phon = phonotephrite, LT = low-TiO_2, HT = high-TiO_2, ign = ignimbrite, aph = aphyric, kna * = $K_2O/(K_2O + Na_2O)$. See Fig. 3 for stratigraphic positions.

Table 4
Sr–Nd isotope data on whole rock B_1 lavas from Jeløya (4a) and clinopyroxene separates from Jeløya and Vestfold. Initial values are estimated, assuming an age of 295 Ma (4b)

(a) Whole rock Sr–Nd data, Jeløya

Sample	Rb/Sr[a]	$^{87}Rb/^{86}Sr$	$^{87}Sr/^{86}Sr_{measured}$	$^{87}Sr/^{86}Sr_{initial}$	ε_{Sr}	Sm/Nd[a]	$^{147}Sm/^{144}Nd$	$^{143}Nd/^{144}Nd_{measured}$	$^{143}Nd/^{144}Nd_{initial}$	ε_{Nd}
ESJ-002	0.0934	0.2703	0.70933	0.70820	57.1	0.187	0.1128	0.51255	0.51233	1.39
ESJ-017	0.0518	0.1498	0.70525	0.70462	6.4	0.209	0.1265	0.51259	0.51234	1.61
ESJ-021	0.0895	0.2589	0.70601	0.70492	10.7	0.203	0.1230	0.51246	0.51223	−0.62
ESJ-057	0.0762	0.2204	0.70662	0.70569	21.6	0.212	0.1279	0.51256	0.51231	1.07
ESJ-080	0.0542	0.1568	0.70544	0.70478	8.7	0.200	0.1209	0.51259	0.51235	1.84
ESJ-093	0.0419	0.1212	0.70591	0.70540	17.5	0.194	0.1171	0.51267	0.51245	3.68
ESJ-150	0.0339	0.0981	0.70471	0.70430	1.8	0.194	0.1176	0.51262	0.51239	2.57
ESJ-181	0.1047	0.3029	0.70640	0.70513	13.6	0.198	0.1196	0.51251	0.51228	0.39
ESJ-207	0.2070	0.5990	0.70959	0.70708	41.2	0.208	0.1260	0.51254	0.51229	0.66
ESJ-221	0.0922	0.2667	0.70659	0.70547	18.4	0.200	0.1209	0.51250	0.51227	0.18
ESJ-223	0.1408	0.4073	0.70699	0.70528	15.7	0.200	0.1209	0.51246	0.51223	−0.60
ESJ-262	0.0724	0.2093	0.70000	0.69912	−71.7	0.210	0.1267	0.51255	0.51230	0.88
ESJ-305	0.0237	0.0686	0.70502	0.70473	8.0	0.198	0.1196	0.51241	0.51217	−1.64
ESJ-314	0.0768	0.2222	0.70682	0.70589	24.4	0.184	0.1112	0.51259	0.51238	2.28
ESJ-360a	0.0516	0.1493	0.70713	0.70650	33.1	0.202	0.1222	0.51256	0.51232	1.23

(b) Clinpyroxene separate Sr–Nd isotope data

Sample	px type	$^{87}Sr/^{86}Sr_{measured}$	$\varepsilon_{Sr\ measured}$	Sm/Nd[a]	$^{147}Sm/^{144}Nd$	$^{143}Nd/^{144}Nd_{measured}$	$^{143}Nd/^{144}Nd_{initial}$	$\varepsilon_{Nd\ initial}$
Jeløya								
JE 016	green	0.70426	1.3	0.301	0.1817	0.51283	0.51247	4.2
JE 316	green	0.70431	2.0	0.303	0.1834	0.51279	0.51243	3.6
JE 316	brown	0.70476	8.4	0.293	0.1772	0.51271	0.51236	2.1
GUH 1X	green	0.70421	0.6	0.292	0.1763	0.51278	0.51243	3.6
GUH 1X	brown	0.70462	6.5	0.310	0.3103	0.51273	0.51236	2.1
GUH 2X	brown	0.70493	10.9	0.271	0.1638	0.51267	0.51235	1.8
Vestfold-Horten								
F1X	green	0.70468	7.3	0.200	0.1210	0.51264	0.51241	3.0
F1X	brown	0.70446	4.2	0.186	0.1124	0.51264	0.51242	3.2
F3X	green	0.70322	−13.5	0.201	0.1218	0.51271	0.51247	4.2
F3X	brown	0.70346	−10.0	0.190	0.1146	0.51267	0.51244	3.7
FZ1X	green	0.70378	−5.5	0.215	0.1302	0.51282	0.51256	6.0
FZ1X	brown	0.70388	−4.0	0.215	0.1303	0.51280	0.51254	5.7
FAX5	brown	0.70301	−16.5	0.190	0.1151	0.51277	0.51255	5.8
FX1BX	green	0.70373	−6.3	0.279	0.1688	0.51280	0.51247	4.2
FX1BX	brown	0.70374	−6.0	0.264	0.1594	0.51280	0.51249	4.6
FX0X	green	0.70371	−6.5	0.279	0.1689	0.51279	0.51246	4.1
FX0X	brown	0.70372	−6.4	0.264	0.1595	0.51279	0.51248	4.5
FX6X	green	0.70373	−6.2	0.278	0.1682	0.51274	0.51241	3.1
FX6X	brown	0.70414	−0.5	0.276	0.1666	0.51268	0.51236	2.0
F4X	green	0.70358	−8.4	0.287	0.1733	0.51276	0.51242	3.3
F4X	brown	0.70377	−5.7	0.280	0.1695	0.51279	0.51246	4.0
FX5X	green	0.70391	−3.7	0.298	0.1805	0.51287	0.51251	5.1
FX5X	brown	0.70397	−2.8	0.289	0.1749	0.51280	0.51246	4.0

[a] Values from ICPMS measurements of whole-rock powders.

basalts (HT and LT) fall along a different trends from that defined by Vestfold LT basalts (Fig. 5c, d). In K–Nb, Rb–Nb, and K_2O–Na_2O plots, the different groups show wide scatter although the HT and the LT basalts define different domains (Fig. 5e, f).

In Fig. 6, we have plotted primordial mantle (PM)-normalized trace element patterns for the HT and LT basalts from Vestfold and Jeløya B_1 series. For each area, HT and LT samples have been divided into two groups depending on their $K_2O/(K_2O+Na_2O)$ ratio values as this ratio discriminates well between altered and unaltered samples. The most uniform trace element patterns are exhibited by lavas with $K_2O/(K_2O+Na_2O)$ values in the range 0.45–0.60. This group is believed to represent the least altered lavas. Lavas with $K_2O/(K_2O+Na_2O)$ ratios <0.45 or >0.6 show considerable scatter in Ba, Rb, and K compared to other incompatible trace elements (except for Sr) including strong negative Rb and K anomalies, which suggest selective removal of these elements. These groups are believed to include the most altered lavas.

Both the HT and the LT groups are characterized by high La/Yb ratios (Tables 2 and 3, Fig. 6). The least altered HT basalts are mildly depleted in Rb and K relative to other incompatible elements, show the highest enrichment factors for Nb and Ta, and show a general tendency for depletion in Sr and P relative to REE (Fig. 6a, b). The least altered LT basalts are enriched in Ba, Rb, and K relative to other incompatible trace elements (Fig. 6c, d); the highest enrichment factors are exhibited for Ba and Rb. Both positive and negative Sr anomalies occur, which is compatible with the accumulation or removal, respectively, of plagioclase. Like the HT basalts, the LT samples show negative anomalies for P. In general, the HT basalts are depleted in Rb in addition to K and Na, and are enriched in most other incompatible elements (e.g. Th, Nb, LREE = light rare earth elements) relative to the LT basalts although the latter, in general, are less mafic (Figs. 4 and 5). These differences are reflected by aphyric as well as porphyritic samples.

5.4. Sr–Nd isotope compositions

A number of representative B_1 lavas from Jeløya were selected for Sr–Nd isotope analyses (Table 4a). In Fig. 7, these analyses of unleached samples are shown together with Vestfold whole-rock analyses (leached; Neumann et al., 1988, 1990), and clinopyroxene separates (Table 4b). The lavas cover a considerable range in isotope compositions (Table 4a, Fig. 7). When corrected for the assumed age of 295 Ma, the Jeløya lavas exhibit a wide range in initial $^{87}Sr/^{86}Sr$–$^{143}Nd/^{144}Nd$ ratios, 0.7043–0.7082 and 0.51217–0.51245, respectively (ε_{Nd}: +3.7 to −1.6, ε_{Sr}: +1.8 to +41.2). These lavas show no correlation between Sr

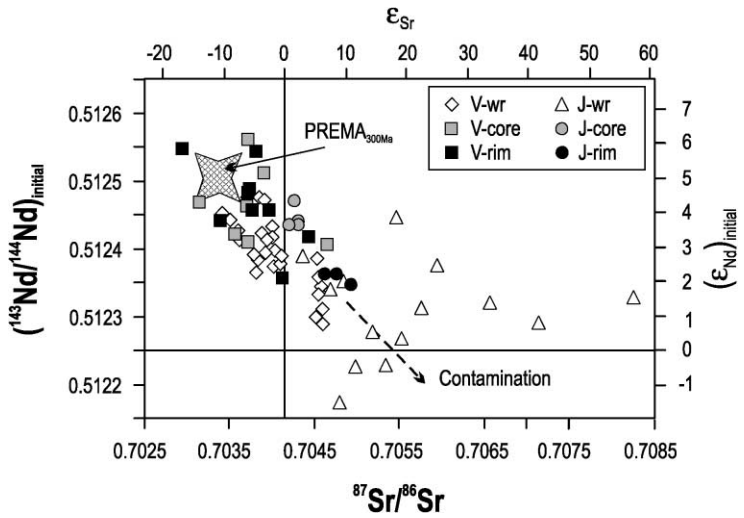

Fig. 7. Initial (295 Ma) Sr–Nd isotopic relations among B_1 basaltic lavas in Vestfold (V) and Jeløya (J). WR = whole rock, core = clinopyroxene phenocryst cores, rim = Ti–augite rims. The position of the PREMA mantle source at 300 Ma (Stein and Hofmann, 1994) is shown.

and Nd isotope signatures. There appears to be a significant difference in isotopic composition between the HT and the LT lavas (ε_{Nd}: +3.7 to −1.6, ε_{Sr}: +1.8 to +57.1). It should be noted that the highest Nd isotope ratios are found among the aphyric samples (both HT and LT). The highest initial ε_{Sr} values (+33 and +57) come from the two analyzed phonotephrites. The difference in isotopic signatures between the Jeløya and the Vestfold lavas is believed to be, at least partly, due to alteration as the Vestfold lavas were leached before Sr–Nd isotopic analysis, whereas the Jeløya samples were not (see discussion below).

Clinopyroxene separates from Jeløya lavas show a more restricted range in isotope compositions (measured $^{87}Sr/^{86}Sr$: 0.7042–0.7049; initial $^{143}Nd/^{144}Nd$: 0.51235–0.51247, assuming an age of 295 Ma; Table 4b). Green pyroxene cores show lower Sr and higher Nd isotopic ratios than brown rims (Fig. 7). Clinopyroxene separates from Vestfold show a somewhat wider range in initial (295 Ma) $^{87}Sr/^{86}Sr$ and $^{143}Nd/^{144}Nd$ ratios, 0.7030–0.7047 and 0.51236–0.51255, respectively. There is a weak tendency for green cores to show lower Sr and higher Nd isotopic ratios than coexisting brown rims. The pyroxene separates fall close to the trend defined by Vestfold lavas (Neumann et al., 1988, 1990).

6. Discussion

The compositional data presented above imply that the B_1 basaltic lavas in Vestfold and Jeløya have been subjected to a series of processes. The effects of the different processes are discussed below, followed by an assessment of the sources from which the primitive magmas were derived.

6.1. Fractional crystallization

As indicated above, all the B_1 lavas in Vestfold and Jeløya carry phenocrysts; the HT basalts have phenocrysts of clinopyroxene and pseudomorphs after olivine, whereas most of the LT series, together with the phonotephrites and ignimbrites, have phenocrysts of plag ± ol ± cpx ± mt ± ap, and relatively low MgO contents (<7 wt.%). This indicates that the parent melts of these lavas have been subjected to significant fractional crystallization. Removal of feldspar, apatite, and/or titanomagnetite is reflected in negative anomalies for Sr, P, Eu, and Ti in samples with relatively low MgO contents. Positive anomalies for these elements, which are observed in some samples, reflect accumulation of one or more of these phases. It should be noticed, however, that although neither plagioclase nor apatite appears as phenocrysts in the HT lavas, the latter shows weak negative Sr and P anomalies in Fig. 6. This suggests that mild Sr and P depletion relative to REE is a primary feature.

Fractionation of the B_1 lavas in Vestfold and Jeløya has led to accumulation of the dense phases olivine, clinopyroxene and titanomagnetite in crustal magma chambers. In the Vestfold–Jeløya area, this must contribute significantly to the positive gravity anomaly found to exist along the Oslo Graben and which is interpreted as the result of emplacement of dense cumulates in the deep or middle crust (e.g. Ramberg and Smithson, 1971; Ramberg, 1976; Neumann et al., 1986; Wessel and Husebye, 1987; Neumann, 1994).

6.2. Stratigraphy

Brögger (1931) proposed that all the lavas in the Vestfold–Jeløya area erupted from a single large volcano that he referred to as the "Hurumvulkan". We disagree with this view. The B_1 lavas define (at least) four distinct groups whose chemical character and stratigraphic relations are incompatible with extrusion from a common magma chamber (Figs. 4–6). As described above, these groups are: (1) high Ti (HT) basalts (TiO_2 > 4.2 wt.%) with relatively high concentrations of most strongly incompatible elements, but negative anomalies for Rb and K, high LREE to HREE ratios; (2) low Ti (LT) basaltic rocks (TiO_2 < 3.7 wt.%), characterized by lower enrichment in strongly incompatible elements relative to MgO contents than the HT basalts, but with positive anomalies for Ba, Rb, and K; (3) phonotephrites highly enriched in most strongly incompatible elements, negative anomalies for Sr, P, and Ti; and (4) ignimbrites with strong negative Sr, P, and Ti anomalies. On the basis of the lava stratigraphy in the different profiles, it is possible to get some information about the relative age relations of these groups and the approximate locations of the eruption centers giving rise to the different groups of Vestfold–Jeløya lavas.

The oldest lavas are the HT basalts (Fig. 3). These are most numerous in the Horten area. From field evidence, the Holmestrand S profile appears to contain fewer HT flows than the Horten profile, and the HT lavas are interfingering with LT lavas. Although the base of HT in Jeløya is below sea level, Downtonian sandstone occurs nearby, suggesting that the hidden part of the HT sequence is unimportant. The HT basalts, thus, seem to be most numerous in the southwestern part of the Vestfold–Jeløya area and probably erupted from a volcanic center located in that vicinity.

The LT lavas consistently make up the upper parts of those profiles where different types of extrusives are present, implying that they are generally younger than the HT basalts. However, interfingering HT and LT lavas in the Holmestrand S profile (but not in the other profiles) imply that the LT lavas originated from a separate extrusive center to the HT lavas and that the LT volcanism must have started before the end of the HT volcanic period. The thickest LT sequences are found to the north and east, suggesting an extrusion center for the LT basalts in that area. The transition from HT to LT volcanism is marked by the extrusion of the relatively evolved phonotephrites and ignimbrites. The phonotephrites in Vestfold and Jeløya are compositionally similar and are markedly different in both major and trace element compositions from the other lavas (Figs. 5–7). We, therefore, believe that the phonotephrites in the different profiles represent the same stratigraphic level. Like the HT basalts, the phonotephrites appear to be more numerous in the southern (Horten, Jeløya Profile I) than in the northern part of the area. The ignimbrites overlying the phonotephrites in the Horten and Jeløya I, II and IV profiles appear to represent a common unit, but it is unclear if the tuff below lava P8b in Holmestrand N (Fig. 3) is related. However, as no other ignimbrites or tuffs have been reported from the area, it seems likely that it is part of this unit. If so, it implies that numerous LT flows erupted between the extrusion of HT and phonotephrite lavas, and that of the ignimbrites in the Holmestrand N area. It is likely that the phonotephrites originate in a third extrusion center. The activity in this center may have ended with the ejection of the highly evolved ignimbrites.

On the basis of the stratigraphic and chemical relations between the different lava series, we conclude that at least three eruption centers were in operation during the B_1 period in the Vestfold–Jeløya area. Thus, the oldest center, giving rise to HT basalts, was most likely located in the southwestern part of the area. Another center, or centers, one of which was located in the northern or northeastern part of the area and giving rise to LT lavas, became active, while the HT center was still in operation. The phonotephrites most likely erupted from a separate center in the southwest during the earliest part of LT volcanism. The ignimbrites may represent highly evolved magmas ejected from the same center. These conclusions are in agreement with those of Schou-Jensen and Neumann (1988).

Gradual upwards decreases in MgO, interrupted by abrupt increases in MgO, observed locally among both HT and LT lavas, are compatible with the results of fractional crystallization in periodically refilled magma chambers. Local, gradual upwards increases in MgO may result from continuous inflow of mafic magma that mixes with somewhat more evolved magma already present in the magma chamber, where inflow of mafic magma dominates over fractional crystallization. Significant decreases in MgO content from one lava to the next probably reflect periods dominated by closed-system fractional crystallization (no significant inflow of mafic magma nor eruptions).

It is to be noticed that although only LT lavas have so far been analyzed among younger basaltic lavas inside the Vestfold rhomb porphyry sequence (Table 1), both HT and LT lavas are present among the younger basalt series in Krokskogen further north (Larsen, 1978; Dunworth, unpublished data). This means that both HT and LT magmas were available over a long period of time.

6.3. Alteration of magmatic trace element signatures

There is ample evidence that the Vestfold and Jeløya lava sequences are affected by alteration. Olivine is generally completely replaced by alteration products, plagioclase is commonly sericitized, and secondary sphene, calcite, and haematite are commonly observed in the groundmass, particularly, in samples from Jeløya (Schou-Jensen and Neumann, 1988).

Alteration is also reflected in isotope and trace element relations. The Jeløya whole-rock series exhibits a wide range in Sr isotope ratios for samples with

similar Nd isotope ratios, an effect seen to a lesser extent in the Vestfold lavas and in the Vestfold and Jeløya clinopyroxene separates (Fig. 7). The scatter seen among the Jeløya whole-rock data is a typical result of alteration in the presence of seawater or meteoric water. Furthermore, the rocks show restricted ranges in ratios between elements that are not easily mobilized during alteration (e.g. La/Nb, Th/Nb, La/Sm), but wide scatters in the values of ratios involving elements easily mobilized (Rb, K, Na; Fig. 5) and in $K_2O/(K_2O+Na_2O)$ ratios (0.1–0.8). In order to differentiate between the rocks with varying degrees of alteration, the lavas were divided into groups of similar $K_2O/(K_2O+Na_2O)$ ratios, and the ranges in values in mobile/immobile element ratios within each group were compared. We found that the mobile/immobile element ratios were least variable within the $K_2O/(K_2O+Na_2O)$ range 0.45–0.60, whereas rocks with $K_2O/(K_2O+Na_2O)$ values below 0.45 and above 0.6 show large variations. We, therefore, conclude that the range 0.45–0.6 is close to, or overlaps, the original $K_2O/(K_2O+Na_2O)$ range. Mobilization of potassium is typical of subaerial weathering.

The wide scatter in $K_2O/(K_2O+Na_2O)$, Rb/Nb, and K/Nb values is, thus, interpreted as the result of trace element mobilization in connection with alteration processes. However, the systematic differences in trace element patterns, including K/Nb and Rb/Nb ratios, between the HT and the LT lava groups (Fig. 5) appear not to be related to alteration processes. The effects of alteration, thus, appear to be superimposed on prealteration contrasts in trace element characteristics between the two groups.

6.4. Crustal contamination

The storage of hot, mafic magmas in crustal magma chambers may easily lead to interaction with the surrounding crustal rocks. This has clearly also happened to the melts which gave rise to the Vestfold–Jeløya lavas. In Fig. 8, Nb/Pb ratios are plotted against Nb concentrations. Hofmann et al. (1986) have shown that the Nb/U and Ce/Pb ratios are uniform in uncontaminated basaltic lavas from different tectonic settings (ca. 50 and 20–30, respectively). Crustal rocks have significantly lower ratios and are generally rich in these elements; the effects of crustal

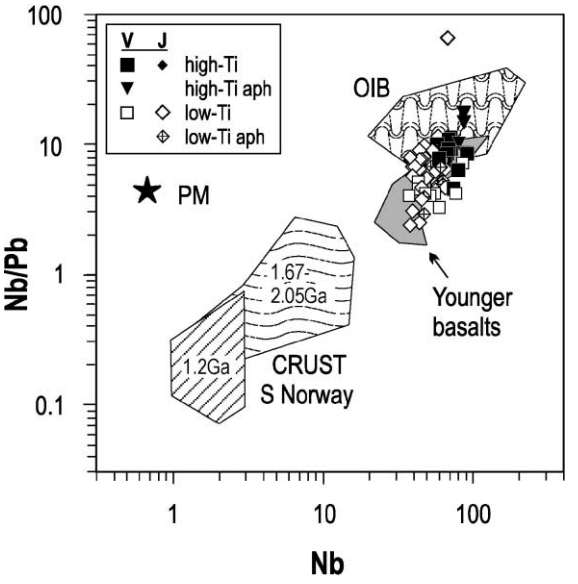

Fig. 8. Nb/Pb–Nb relations in basaltic B_1 lavas from Vestfold (V) and Jeløya (J), compared to ocean islands basalts assumed to have retained their mantle signatures (OIB: Halliday et al., 1995), primordial mantle (PM: McDonough and Sun, 1995), and the ranges of ≈ 1200 and 1.67–2.05-Ga-old crustal rocks from the amphibolite-to-granulite facies Bamble sector, southern Norway (Knudsen et al., 1997; Knudsen and Andersen, 1999). Also, the compositions of younger basaltic lavas in Vestfold and Krokskogen are shown for comparison (Sundvoll, unpublished data; this study). *Aph*: aphyric; *phonoteph*: phonotephrites.

contamination may, therefore, be easily detected in these ratios. Nb, REE, and Pb are relatively immobile during alteration processes (e.g. Henderson, 1982), whereas U is easily mobilized. As alteration has affected the Vestfold–Jeløya B_1 basalts to different degrees and as few data are available on Ce in crustal rocks from southern Norway, we have used the Nb–Pb relations to investigate contamination.

The Vestfold–Jeløya lavas define a trend from ratios typical of the mantle, towards the general domain of amphibolite-to-granulite facies Proterozoic crustal rocks in the Bamble sector, S Norway (Knudsen and Andersen, 1999), which are likely to be representative of the crustal basement beneath the Vestfold and Jeløya lavas (Fig. 1). This suggests crustal contamination. On average, the LT basalts appear to be more contaminated than the HT basalts. Younger basalts (B_2 and B_3) from Vestfold and Krokskogen further north (Fig. 1) show an even more extensive trend towards the crustal average (Sundvoll, unpublished data, 2000). This

may reflect an increasing degree of contamination with time, as the crust in the Oslo Region became progressively heated by intrusions of hot mafic magmas or, alternatively, longer magma residence times in the crust in the northern than in the southern part of the rift due to less marked extension across the rift (Sundvoll and Larsen, 1994).

Isotope data also support the involvement of crustal contamination. The Vestfold B_1 lavas define a rough trend ranging from a moderately depleted position in the upper left quadrant of the $^{87}Sr/^{86}Sr-^{143}Nd/^{144}Nd$ anti-correlation plot towards more enriched compositions (Fig. 7). This was also noticed by Neumann et al. (1988) and Anthony et al. (1989), who interpreted the trend to be the result of crustal contamination. The wide range in Sr isotopic ratios among the unleached Jeløya basalts is most likely the result of alteration. The wide range in Nd isotopic ratios exhibited by the Jeløya basalts suggests that prior to contamination (which mainly affected the Sr isopotic ratios), these lavas may have defined a trend similar to the Vestfold trend.

The new Sr–Nd isotope data obtained from acid-leached clinopyroxene mineral separates (Fig. 7) also help to constrain the influence and timing of crustal contamination in these samples. The clinopyroxene phenocrysts were separated into magnesian diopside cores and Ti–augite rims from each sample, where appropriate. It is assumed that the early formed cores record the most primitive isotopic signatures available of the magmas from which they crystallized. As can be seen in Fig. 7, most of the core compositions show relatively depleted isotopic signatures, suggesting that some of the more enriched signatures of the Ti–augite rims that are believed to have crystallized at relatively shallow depths, as well as many of the whole-rock compositions, reflect the signatures of later-stage crustal contamination effects.

The main Vestfold–Jeløya trend reflects the influence of (at least) two contributing components with different isotopic compositions. The depleted end of the mixing trend points towards a moderately depleted mantle source corresponding to the 300 Ma position of the PREvalent MAntle (PREMA) reservoir of Stein and Hofmann (1994; $[^{143}Nd/^{144}Nd]_{300\ Ma} \approx 0.5125$, or $\varepsilon_{Nd} \geq +5$, and $\varepsilon_{Sr\ 300\ Ma} \approx -11$). Some clinopyroxene separates have more depleted isotope signatures than $PREMA_{300\ Ma}$, suggesting that there may have been some contribution from a more depleted source. The other end points towards a mildly enriched source, which may well represent upper crustal contamination as indicated by the trace element and isotope data although a contribution from an enriched mantle source cannot be excluded in some cases, particularly, in the LT lavas, as will be discussed later. It should be noted that the earliest pyroxene cores from the Jeløya lavas show more enriched isotopic compositions than those of similar pyroxenes from the Vestfold lavas. This suggests differences in mantle sources or degree of lithospheric contamination in the early stages of magma crystallization and provides additional evidence for separate plumbing systems in Vestfold and Jeløya. Finally, the lavas have $^{143}Nd/^{144}Nd$–Ce/Pb relations intermediate between those characteristic of the mantle and the crust (Fig. 9). Also, the scatter in ratios between strongly incompatible elements not easily mobilized by alteration processes (e.g. Th/Nb, La/Nb, Zr/Nb; Fig. 5) may, at least partly, be due to crustal contamination.

Neumann et al. (1988, 1990) proposed that the isotopic compositions of B_1 lavas from Vestfold, and trachyandesitic extrusive and intrusive rocks (rhomb-

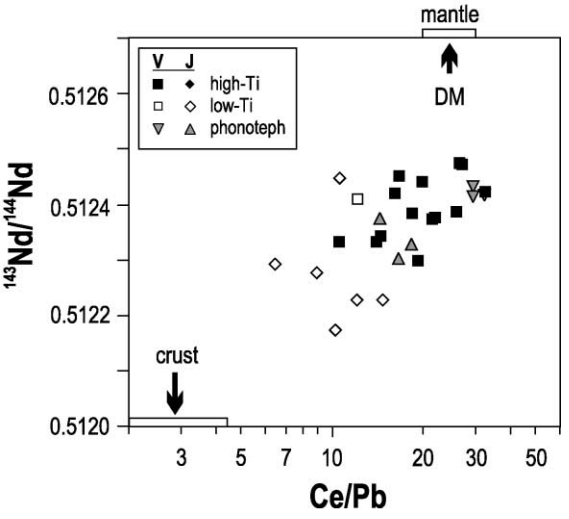

Fig. 9. $^{143}Nd/^{144}Nd$–Ce/Pb for B_1 lavas from Vestfold (V) and Jeløya (J) showing indications of crustal contamination. The Ce/Pb range of mantle and crustal sources are the same as in Fig. 8, arrows indicate the high and low $^{143}Nd/^{144}Nd$ ratios typical of the depleted mantle and the crust, respectively. *Aph*: aphyric; *phonoteph*: phonotephrites.

porphyry lavas and larvikites) in the Oslo rift reflect derivation of their initial melts from a mildly depleted mantle source (ε_{Nd} and ε_{Sr} of +4.1 and −10, respectively) and contamination to different degrees in the lower crust. The data presented in this paper suggest that the basaltic magmas, which reached the surface directly, were only contaminated during the final stages of their crustal traverse; lower-crustal magma chambers were subsequently established from which the more evolved derivatives were later erupted.

6.5. Melting processes

Although the melts, which gave rise to the HT and LT lavas, have been affected by crustal contamination, fractional crystallization, mixing, and post-magmatic alteration processes, some geochemical signatures are believed to represent mantle source(s). Among these are the isotopic signatures preserved of the green cores in the clinopyroxene phenocrysts (Fig. 7). These cores may represent mantle neoblasts coated by Ti–augite formed from the host magma (Kirstein, personal communication, 2000; Dunworth, unpublished data), or they may have crystallized from primary magma (Fig. 7).

Like continental rift magmatism, in general, the Vestfold and Jeløya B_1 lavas exhibit PM-normalized trace element patterns characterized by enrichment in strongly incompatible elements relative to moderately incompatible ones including strong enrichment in LREE relative to HREE (Tables 2 and 3, Fig. 6). However, the concentrations of Y and HREE in the most mafic lavas are significantly lower than in average N-MORB (using data from, e.g. Sun and McDonough, 1989). This clearly reflects generation of the initial melts by partial melting in the presence of residual garnet. The depletion in Rb and K relative to Ba, Th, and U, which characterizes the least altered HT basalts, and positive anomalies for Ba, Rb, and K in the LT basalts are believed to be primary features, as is the stronger enrichment in highly incompatible elements in the HT than in the LT basalts (Fig. 6). We also believe that the observed systematic differences in some ratios between strongly incompatible elements that are not easily mobilized during post-magmatic alteration (e.g. La/Sm and Zr/Nb; Fig. 5c, d) are primary features. Because of the complex post-melting processes that have affected the rocks, it is difficult to judge if the initial melts had similar isotopic signatures or not.

The compositions of the primary melts that gave rise to the Oslo rift magmatism are currently unknown. However, some information may be obtained by compensating for fractional crystallization. As indicated above, all the Vestfold–Jeløya B_1 lavas, including the "least evolved" ones, have a prehistory of fractional removal of ol and ol + cpx, some contain large amounts of olivine and clinopyroxene phenocrysts and have compositions indicating accumulation of these phases. Spinel is commonly observed as microphenocrysts in olivine in alkaline rock series and is clearly an early phase in many such rocks (e.g. Dunworth and Wilson, 1998; Neumann et al., 1999). However, spinel is sufficiently rare in comparison to the abundance of other phases in the Vestfold–Jeløya samples to make no significant difference to the rather crude calculations outlined below. We, thus, assume that the HT basalts have a history of fractional crystallization of *olivine* (stage FCI) followed by *olivine + clinopyroxene* (stage FCII). The phenocryst assemblage in the HT lavas (olivine and clinopyroxene) implies that the magmas were in stage FCII when extruding. The most MgO-rich aphyric HT lava (F17, ≈ 8 wt.% MgO; Table 5) is used as the resultant melt in the model. The

Table 5
Compositions used to calculate trends FCI and FCII in Fig. 10

Phase Sample	Start compositions			Estimated melts	
	Rock	cpx	ol	FCI	FCII
	F17	FA3	Hypo.		
SiO_2	44.50	50.47	40.01	43.15	43.56
TiO_2	4.82	1.69		3.37	3.01
Al_2O_3	9.28	2.72		6.50	5.75
FeO	11.88	7.05	14.35	12.62	12.27
MnO	0.15	0.14		0.11	0.10
MgO	8.11	15.67	45.64	19.37	20.79
CaO	11.24	21.55		7.87	8.50
Na_2O	1.59	0.62		1.11	1.00
K_2O	1.78			1.25	1.06
P_2O_5	0.73			0.51	0.43

The trends estimate more primitive melts by compensation for removal of olivine (FCI) or olivine + clinopyroxene in the proportion 20:80 (FCII). The low TiO_2 endpoints of the FCI and FCII trends represent hypothetical primary melts which would give rise to melts of F17 compositions after "30%" fractional crystallization; these compositions are listed below as "Estimated melts". Hypo. = hypothetical. See text for further explanation.

compositions of clinopyroxenes in a number of the Vestfold lavas are given by Øverli (1985). For our calculations, we chose the core composition of clinopyroxene in lava FA3 (Table 5), which is somewhat more magnesian than groundmass clinopyroxene (15.03 wt.% MgO) in the aphyric lavas F13–F17. Because of alteration, we do not have analyses of olivine in the most primitive lavas. For olivine, we have, therefore, estimated an early/primitive composition of Fo_{85}, supposed to be in equilibrium with clinopyroxenes with Mg# in the high 80s. As we do not know the total extent of crystallization that led from the initial magma to form the F17 melt nor the extent of crystallization at each stage leading from the primary melt to the F17 stage, we list different examples in Table 5; backtracking towards the initial melt composition by adding olivine (FCI), or olivine and clinopyroxene in the cotectic proportion 20:80 (FCII). As the estimates are very crude, we have made no attempts to compensate for changes in the compositions of the crystallizing phases during the fractionation sequence. In spite of this, we have listed the compositions of two estimated melts (Table 5) that would give rise to the F17 composition by 30% fractional crystallization. The results (Table 5, Fig. 10) show that fractionation of ol or ol + cpx increases the concentration of TiO_2 in the residual melt, whereas the change in the TiO_2/Al_2O_3 ratio is negligible. It may, therefore, be safely assumed that the initial melts that gave rise to the HT basalts were very rich in TiO_2, probably >4.0 wt.%. This is also backed up by the fact that the spidergrams have gentle curves over the MREE–Ti–Zr–Hf section and lack positive Ti spikes.

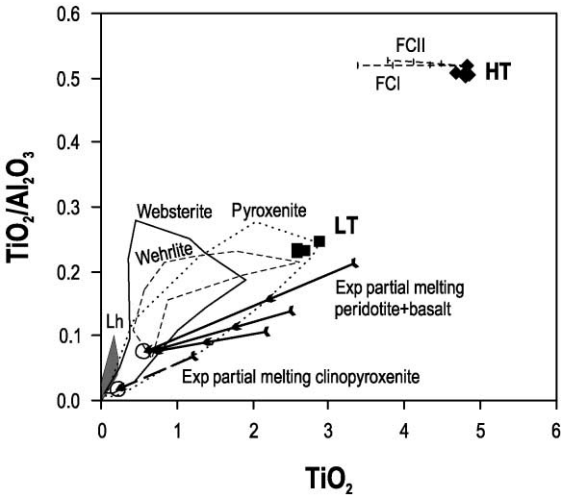

Fig. 10. TiO_2/Al_2O_3 ratios plotted against TiO_2 for aphyric HT lavas in Vestfold (HT) and mafic, aphyric LT lavas in Jeløya (LT). The figure shows two separate trends of increasing TiO_2 and near constant TiO_2/Al_2O_3 with increasing degree of fractional crystallization; FCI: removal of olivine; FCII: removal of the assemblage $olivine_{20}$ + $clinopyroxene_{80}$; tic-marks for every 10% fractional crystallization. Heavy lines show the TiO_2/Al_2O_3–TiO_2 relations in glasses produced in partial melting experiments with lherzolite (Kinzler, 1997; Robinson et al., 1998) and peridotite + basalt (Kogiso et al., 1998) as starting materials; the highest TiO_2 contents and TiO_2/Al_2O_3 ratios occur at very low degrees of partial melting (indicated by the back-ends of the arrows), the arrows point in the directions of progressive partial melting. The fields of lherzolite and harzburgite xenoliths and massifs (gray), pyroxenites (dotted line), websterites (full line) and wehrlites (dashed line) in continents and ocean islands are shown for comparison (Neumann, 1991; data compilation by Hirschmann and Stolper, 1996). See text for further discussion.

The high TiO_2 contents in the HT series are not compatible with partial melting of spinel or garnet peridotite. Average compositions of the subcontinental lithospheric mantle in different areas, estimated on the basis of peridotite xenoliths and massifs, show TiO_2 concentrations up to 0.21 wt.% (Griffin et al., 1999). Partial melting experiments using peridotite as starting materials have shown that TiO_2 becomes most highly enriched in the melts formed by very low degrees of partial melting (e.g. Mysen and Kushiro, 1977; Jaques and Green, 1980; Falloon and Green, 1987; Baker and Stolper, 1994; Falloon et al., 1997; Kinzler, 1997; Kogiso et al., 1998; Robinson et al., 1998). However, even experiments on peridotite with 0.17 wt.% TiO_2 (Fig. 10) gave a maximum of 1.3 wt.% TiO_2 in melts formed at near-solidus temperatures (melt fraction < 1%), and the TiO_2/Al_2O_3 ratio did not exceed 0.7 (Robinson et al., 1998). It seems clear that a source highly enriched in Ti and other HFSE relative to peridotites must have been involved in the generation of the HT basalts. Ti-rich mantle rocks comprise clinopyroxenites, wehrlites, websterites, and amphibolites (Fig. 10). These rock types (referred to below as clinopyroxenites) are commonly enriched in TiO_2, Al_2O_3 and other incompatible elements compared to lherzolites and harzburgites and have higher TiO_2/Al_2O_3 ratios (Fig. 10); they may contain quite Ti-rich clinopyroxene, kaersutitic amphibole, and/or phlogopite, and include apatite, rutile and ilmenite as accessory phases (e.g. Foley,

1992; Witt-Eickschen and Harte, 1994; McPherson et al., 1996; Woodland et al., 1996; Kopylova et al., 1999; Ho et al., 2000; Downes, 2001). Furthermore, the HT basalts have very high CaO/Al_2O_3 ratios (1.4–1.8 in the most magnesian basalts; Fig. 11), which, according to Sigurdsson et al. (2000), indicate a pyroxenitic or wehrlitic mantle source component. At pressures below about 3 GPa, clinopyroxenites have lower solidi than peridotite (e.g. Hirschmann and Stolper, 1996, and references therein). Partial melting experiments on synthetic clinopyroxenite (Hirschmann and Schiano, 1999) and on mixtures of peridotite and basalt (Kogiso et al., 1998) show significant enrichment in TiO_2 contents and TiO_2/Al_2O_3 ratios in melts relative to starting materials (Fig. 10). The starting materials of these experiments lie in the lower part of the TiO_2–TiO_2/Al_2O_3 field of natural clinopyroxenites, and the melts produced are Ti-poor relative to the HT basalts. However, the experiments imply that partial melting of Ti-rich clinopyroxenites may well produce melts with TiO_2 contents and TiO_2/Al_2O_3 ratios similar to those of the HT basalts. Finally, interstitial glasses in low Mg spinel wehrlite, dunite, and clinopyroxenite xenoliths (Fo_{76-83} in olivine) with Ti-rich clinopyroxene and spinel from Hierro, Canary Islands (Neumann, 1991) have chemical characteristics similar to those of the HT basalts (ca. 45 wt.% SiO_2, ≤ 5.6 wt.% TiO_2, ≤ 2.2 wt.% P_2O_5, $TiO_2/Al_2O_3 = 0.2–0.4$; Neumann, unpublished data).

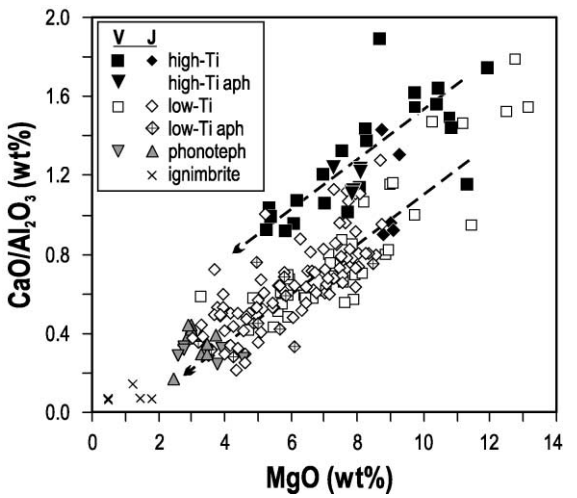

Fig. 11. CaO/Al_2O_3 ratios plotted against MgO for B_1 lavas in Vestfold (V) and Jeløya (J). The figure shows two separate trends of decreasing CaO/Al_2O_3 ratios with decreasing MgO that is increasing degree of fractional crystallization, showing lower CaO/Al_2O_3 ratios at any given MgO concentration in the LT than in the HT lavas. *Aph*: aphyric; *phonoteph*: phonotephrites.

The data presented above strongly suggest that partial melting of nonperidotitic source material containing significant amounts of garnet, amphibole, phlogopite, apatite, and clinopyroxene were involved in the generation of the HT basalts in view of their unusually high HFSE and P content and relatively steep REE pattern. Melting of mixed clinopyroxenite–peridotite mantle sources has previously been proposed to explain the isotopic and chemical heterogeneities of some basalt series (e.g. Foley, 1992; Sigmarsson et al., 1998; Lassiter et al., 2000; Sigurdsson et al., 2000). Such a model may also explain many of the compositional relationships between the HT and LT basalts.

Higher CaO/Al_2O_3 ratios for similar MgO contents in the HT as compared to the LT basalts (Fig. 11) strongly suggest a source richer in clinopyroxene for the former than for the latter. Low Ba–Rb–K concentrations combined with high concentrations in other incompatible elements in the HT basalts as compared to the LT basalts (Figs. 4–6) are compatible with progressive partial melting of phlogopite-bearing source material(s). Published mineral/melt partition coefficients imply that Ba, Rb, and K are compatible in phlogopite, but incompatible in non-hydrous mantle minerals (e.g. LaTourette et al., 1995; Chazot et al., 1996; Foley et al., 1996; Schmidt et al., 1999); only Ba and K are compatible in mantle amphibole (Chazot et al., 1996; Bottazzi et al., 1999; Tiepolo et al., 2000). The early stages of melting of fertile peridotite with clinopyroxenite veins or layers would, to a large degree, occur in the veins and in the adjacent metasomatized peridotite, causing solid solution melting in many of the fertile silicate phases (Foley, 1992) and removing apatite, but leaving garnet and phlogopite in the peridotite-vein residue. This stage would give rise to highly P–HFSE–REE-enriched HT melts with high TiO_2/Al_2O_3 and CaO/Al_2O_3 ratios, whereas trace elements compatible with garnet, clinopyroxene, and phlogopite became relatively enriched in the residual solid. Subsequent partial melting would involve a mixture of residual vein minerals and wall-rock peridotite, removing remaining phlogopite and much of

the residual garnet, giving rise to LT melts more enriched in Ba, Rb, and K, and less enriched in other incompatible elements than the HT melts, and with shallower REE patterns.

It is interesting to note that the trace element patterns of the least altered HT and the LT lava groups (Fig. 6) resemble those of HIMU and the EMI end-member trace element compositions, respectively, as outlined by Weaver (1991) (depletion in Rb and K relative to Ba, Th, and U, and high enrichment in Nb and Ta in the HT basalts; positive anomalies for Ba, Rb, and K in the LT basalts). We, thus, propose that basalts with HIMU- and EMI-type trace element compositions may arise through progressive partial melting of a mixed source although we recognize that the isotopic signatures of the Vestfold–Jeløya basalts do not match those of the HIMU end member (Dunworth et al., in preparation).

6.6. Mantle sources

It was argued above that a mixed source consisting of peridotite with veins or layers of garnet–apatite–oxide–phlogopite-bearing clinopyroxenite were involved in the generation of the HT and LT magmas. Clinopyroxenite veins and layers are common features in continental ultramafic massifs (e.g. Downes, 2001, and references therein), and are postulated for the convecting and the lithospheric mantle (e.g. Allègre and Turcotte, 1986; Foley, 1992; Hirschmann and Stolper, 1996). As indicated above, the upper part of the Vestfold–Jeløya Nd–Sr array falls to the low $^{143}Nd/^{144}Nd$–$^{87}Sr/^{86}Sr$ side of the main mantle array (Fig. 7), assumed to represent the isotopic signatures of the sublithospheric mantle over time (Stein and Hofmann, 1994; Zindler and Hart, 1986; Hofmann, 1997). Given the depleted nature of the isotopic signatures, but enriched trace element signatures seen in the most primitive lavas, we propose that the source of the Vestfold–Jeløya lavas was located at the base of the lithosphere and had recently been subjected to an episode of metasomatism from enriched asthenospheric melts. Thus, the main component of the source is essentially asthenospheric material recently transported into the base of the lithosphere. A source physically located in the lower part of the mantle lithosphere is in agreement with the above conclusions that the source consists of fertile peridotite with garnet clinopyroxenite veins. A lithospheric source for the Vestfold–Jeløya B_1 lavas was also proposed by Neumann et al. (1990). Similar models have been proposed for a number of rift environments—Rhinegraben (Wilson et al., 1995), East African Rift system (Furman and Graham, 1999), Kola Peninsula (Dunworth and Bell, 2001)—where small-degree partial melts with depleted isotopic signatures and enriched trace element signatures are found, indicating recent source metasomatism. Dunworth and Bell (2001) also invoked the PREMA source component for the Devonian mantle plume underneath the Kola Peninsula and a similar source may also be responsible for the Dneiper–Donets Rift magmatism of similar age (Wilson and Lyashkevich, 1996) also within the Baltic Shield.

The trace element data described earlier indicate that the Vestfold–Jeløya melts were derived from within the garnet stability field. At solidus temperatures, garnet clinopyroxenite is stable at pressures above about 1.5 GPa (e.g. Irving, 1974), i.e. at depths greater than ca. 45 km. Seismic studies give a present–day lithospheric thickness of 110 km beneath northern Denmark, which increases northwards both along the Oslo rift and away from the rift area (Calcagnile, 1982). Recent modeling has assumed a thickness of the lithosphere of 120–130 km at the onset of the rifting period (Pascal, personal communication, 2000). This means that both garnet clinopyroxenite and garnet peridotite were stable at solidus temperatures within the lower parts of the lithospheric mantle during the Oslo rifting event.

6.7. European Permo-Carboniferous magmatism

The lavas found in the Oslo rift contain the most extensive suite of primitive basalts found in the large European Permo-Carboniferous rifting event. As such, they provide a unique opportunity to study the composition of the parental lavas and mantle sources that gave rise to the enormous volumes of magma erupted and emplaced across Europe during this time. The reoccurrence of the PREMA isotopic signature of Stein and Hofmann (1994), seen in so many major igneous events around the world over time and in plume-related Devonian magmatism within the Baltic Shield (Dunworth and Bell, 2001), suggests that the dominant trace element-enriched, isotopically depleted component seen in the Vestfold–Jeloya lavas may also

be derived from material from a similar mantle plume impinging on the base of the European lithosphere.

7. Conclusions

The following conclusions have been reached with respect to the origin and evolutionary history of the B_1 basaltic lavas in Vestfold and Jeløya in the central part of the Oslo rift.

(1) The B_1 lavas in Vestfold and Jeløya comprise four main groups: HT basalts ($TiO_2 > 4.2$ wt.%), LT basaltic rocks ($TiO_2 < 3.7$ wt.%), phonotephrites, and ignimbrites. The chemical characteristics and stratigraphic relations of these groups are incompatible with extrusion from a common magma chamber.

(2) The preserved lava sequences in Vestfold and Jeløya represent interfingering of lavas from at least three eruption centers. The oldest center, giving rise to HT basalts, was most likely located in the southwestern part of the area. Another center (or centers) giving rise to LT basalts was located in the northern part of the area. The phonotephrites (and possibly the ignimbrites) most likely erupted from a separate center in the southwest during the earliest part of LT volcanism.

(3) During ascent, the magmas were subjected to different degrees of fractional crystallization, mixing between evolved and mafic magma, and upper crustal contamination with material similar to that exposed in the Bamble sector to the west of the rift.

(4) After extrusion, the lavas suffered post-magmatic alteration that led to mobilization, primarily of Rb, U, and K, and increased $^{87}Sr/^{86}Sr$ ratios through introduction of meteoric water (or seawater).

(5) The high TiO_2 contents and high TiO_2/Al_2O_3 ratios of the HT series are not compatible with partial melting of spinel or garnet peridotite, but requires the involvement of Ti-rich source rocks such as clinopyroxenites, wehrlites, websterites, and amphibolites.

(6) The base of the lithosphere, containing veins of enriched material derived from a recently enriched source within the asethenospheric mantle below, is believed to be the most likely source for the Vestfold–Jeløya lavas. Progressive melting of this complex source initially produced magnesian lavas with high REE and HFSE contents, followed by less enriched, more voluminous lavas.

(7) The isotopic compositions of the early basalts suggest that they were derived from an isotopically depleted source similar to the PREMA source of Stein and Hofmann (1994). Contribution of older lithospheric material to the later basalts produced more enriched Sr–Nd isotopic signatures.

Acknowledgements

The authors would like to thank Tom Andersen, Gareth Davies, Toril Enger, Gunborg Fjeld, Mélanie Griselin, and Linda Kirstein for technical assistance. This work has been carried out as part of an EU-funded TMR network: Permo-Carboniferous Rifting in Europe (project ERBFMRXCT960093). This paper has improved through constructive criticism from Reidar G. Trønnes and Elisabeth Anthony.

References

Allègre, C.J., Turcotte, D., 1986. Implications of a two-component marble-cake mantle. Nature 323, 123–127.

Anthony, E.Y., Segalstad, T.V., Neumann, E.-R., 1989. An unusual mantle source region for nephelinites from the Oslo rift, Norway. Geochim. Cosmochim. Acta 53, 1067–1076.

Baker, M.B., Stolper, E.M., 1994. Determining the composition of high-pressure mantle melts using diamond aggregates. Geochim. Cosmochim. Acta 58, 2811–2827.

Benek, R., Kramer, W., McCann, T., Scheck, M., Negendank, J.F.W., Korich, D., Huebscher, H.-D., Bayer, U., 1996. Permo-Carboniferous magmatism and related subsidence of the NE German Basin. Tectonophysics 266, 379–404.

Bottazzi, P., Tiepolo, M., Vannucci, R., Zanetti, A., Brumm, R., Foley, S.F., Oberti, R., 1999. Distinct site preferences for heavy and light REE in amphibole and the prediction of $^{Amph/L}D_{REE}$. Contrib. Mineral. Petrol. 137, 36–45.

Brögger, W.C., 1931. Die Eruptivgesteine des Oslogebietes. V. Der grosse Hurumvulkan. Skr. Nor. Vidensk.-Akad. [Kl.] 1: Mat.-Naturvidensk. Kl. 1930 (6), 146 pp.

Calcagnile, G., 1982. The lithosphere–asthenosphere system in Fennoscandia. Tectonophysics 90, 19–35.

Chazot, G., Menzies, M.A., Harte, B., 1996. Determination of partition coefficients between apatite, clinopyroxene, amphibole, and melt in natural spinel lherzolites from Yemen: implications for wet melting of the lithospheric mantle. Geochim. Cosmochim. Acta 60, 423–437.

Downes, H., 2001. Formation and modification of the shallow subcontinental lithospheric mantle: a review of geochemical evidence from ultramafic xenolith suites and tectonically emplaced ultramafic massifs of Western and Central Europe. J. Petrol. 42, 233–250.

Dunworth, E.A., Bell, K., 2001. The Turiy Massif, Kola Peninsula, Russia: isotopic and geochemical evidence for multi-source evolution. J. Petrol. 42, 377–405.

Dunworth, E.A., Wilson, M., 1998. Olivine melilitites of the SW German Tertiary Volcanic Province: mineralogy and petrogenesis. J. Petrol. 39, 1805–1836.

Falloon, T.J., Green, D.H., 1987. Anhydrous partial melting of MORB pyrolite and other peridotite compositions at 10 kbar; implications for the origin of primitive MORB glasses. Mineral. Petrol. 37, 181–219.

Falloon, T.J., Green, D.H., O'Neill, H.St.C., Hibberson, W.O., 1997. Experimental tests of low degree peridotite partial melt compositions: implications for the nature of anhydrous near-solidus peridotite melts at 1 GPa. Earth Planet. Sci. Lett. 152, 149–162.

Foley, S.F., 1992. Vein-plus-wall-rock melting mechanisms in the lithosphere and the origin of potassic alkaline magmas. Lithos 28, 435–453.

Foley, S.F., Jackson, B.J., Greenough, J.D., Jenner, G.A., 1996. Trace element partition coefficients for clinopyroxene and phlogopite in alkaline lamprophyre from Newfoundland by LAM-ICP-MS. Geochim. Cosmochim. Acta 60, 629–638.

Furman, T., Graham, D., 1999. Erosion of lithospheric mantle beneath the East African Rift system; geochemical evidence from the Kivu volcanic province. Lithos 48, 237–262.

Griffin, W.L., O'Reilly, S.Y., Ryan, C.G., 1999. The composition and origin of sub-continental lithospheric mantle. In: Fei, Y., Bretka, C.M., Mysen, B.O. (Eds.), Mantle Petrology: Field Observations and High Pressure Experimentation: A Tribute to Francis R. (Joe) Boyd. Geochem. Soc., Spec. Publ., vol. 6, pp. 13–45.

Halliday, A.N., Lee, D.C., Tommasini, S., Davies, G.R., Paslick, C.R., Fitton, J.G., James, D.E., 1995. Incompatibel trace elements in OIB and MORB and source enrichment in the sub-oceanic mantle. Earth Planet. Res. Lett. 133, 379–395.

Henderson, P., 1982. Inorganic Geochemistry Pergamon, Oxford, 353 pp.

Hirschmann, M.M., Schiano, P., 1999. Experimental study of partial melts of clinopyroxenite and the origin of ultra-calcic melt inclusions (abstract). Ninth Annual International Goldschmidt Conference, Cambridge, MA.

Hirschmann, M.M., Stolper, E.M., 1996. A possible role for garnet pyroxenite in the origin of 'garnet signature' in MORB. Contrib. Mineral. Petrol. 124, 185–208.

Ho, K.-S., Chen, J.-C., Smith, A.D., Juang, W.-S., 2000. Petrogenesis of two groups of pyroxenite from Tungchihsu, Penghu Islands, Taiwan Strait: implications for mantle metasomatism beneath SE China. Chem. Geol. 167, 355–372.

Hofmann, A.W., 1997. Mantle geochemistry: the message from oceanic volcanism. Nature 385, 219–229.

Hofmann, A.W., Jochum, K.P., Seifart, M., White, W.M., 1986. Nb and Pb in oceanic basalts: new constraints on mantle evolution. Earth Planet. Sci. Lett. 79, 33–45.

Irvine, T.N., Baragar, W.R.A., 1971. A guide to chemical classification of the common volcanic rocks. Can. J. Earth Sci. 8, 523–548.

Irving, A.J., 1974. Geochemical and high pressure experimental studies of garnet pyroxenite and pyroxene granulite xenoliths from the Delegate basaltic pipes, Australia. J. Petrol. 15, 1–40.

Jaques, A.L., Green, D.H., 1980. Anhydrous melting of peridotite at 0–15 kbar pressure and the genesis of tholeiitic basalts. Contrib. Mineral. Petrol. 73, 287–310.

Kinck, J.J., Husebye, E.S., Lund, C.-E., 1991. The south-Scandinavian crust: structural complexities from seismic reflection and refraction profiling. Tectonophysics 189, 117–133.

Kinzler, R., 1997. Melting of mantle peridotite at pressure approaching the spinel to garnet transition: application to mid-ocean ridge basalt petrogenesis. J. Geophys. Res. 102, 853–874.

Knudsen, T.-L., Andersen, T., 1999. Petrology and geochemistry of the Tromøy gneiss complex, South Norway, an alleged example of Proterozoic depleted lower continental crust. J. Petrol. 40, 909–933.

Knudsen, T.-L., Andersen, T., Maijer, C., Verschure, R.H., 1997. Trace-element characteristics and Pb isotopic evolution of metasediments and associated Proterocoic rocks from the amphibolite-to granulite-facies Bamble sector, southern Norway. Chem. Geol. 143, 145–169.

Kogiso, T., Hirose, K., Takahashi, E., 1998. Melting experiments on homogeneous mixtures of peridotite and basalt: application to the genesis of ocean island basalts. Earth Planet. Sci. Lett. 162, 45–61.

Kopylova, M.G., Russell, J.K., Cookenboo, H., 1999. Petrology of peridotite and pyroxenite xenoliths from the Jerico kimberlite: implications for the thermal state of the mantle beneath the Slave Craton, Northern Canada. J. Petrol. 40, 79–104.

Larsen, B.T., 1978. Krokskogen lava area. In: Dons, J.A., Larsen, B.T. (Eds.), The Oslo Paleorift. A Review and Guide to Excursions. Nor. Geol. Unders., vol. 337, pp. 143–162.

Lassiter, J.C., Hauri, E.H., Reiners, P.W., Garcia, M.O., 2000. Generation of Hawaiian post-erosional lavas by melting of a mixed lherzolite/pyroxenite source. Earth Planet. Sci. Lett. 178, 269–284.

LaTourette, T., Hervig, R.L., Holloway, J.R., 1995. Trace element partitioning between amphibole, phlogopite, and basanitic melt. Earth Planet. Sci. Lett. 135, 13–30.

Le Bas, M.J., Le Maitre, R.W., Streckeisen, A., Zanettin, B., 1986. A chemical classification of volcanic rocks based on the total alklai–silica diagram. J. Petrol. 27, 745–750.

Le Maitre, R.W. (Ed.), 1989. A Classification of Igneous Rocks and Glossary of Terms. Blackwell Scientific Publications, London, UK.

MacDonald, R., Gottfried, D., Farrington, M.J., Brown, F.W., Skinner, N.G., 1981. Geochemistry of a continental tholeiitic suite: late Palaeozoic quartz dolerite dykes of Scotland. Trans. R. Soc. Edinburgh: Earth Sci. 72, 57–74.

McDonough, W.F., Sun, S.-S., 1995. The composition of the Earth. Chem. Geol. 120, 223–253.

McPherson, E., Thirlwall, M.F., Parkinson, I.J., Menzies, M.A., Bodinier, J.L., Woodland, A., Bussod, G., 1996. Geochemistry of metasomatism adjacent to amphibole-bearing veins in the Lherz peridotite massif. Chem. Geol. 134, 135–157.

Mearns, E.W., 1986. Sm–Nd ages for Norwegian garnet peridotites. Lithos 19, 269–278.

Mysen, B.O., Kushiro, I., 1977. Compositional variations of coex-

isting phases with degree of melting of peridotite in the upper mantle. Am. Mineral. 62, 843–865.
Neumann, E.-R., 1991. Ultramafic xenoliths from Hierro, Canary Islands: evidence for melt infiltration in the upper mantle. Contrib. Mineral. Petrol. 106, 236–252.
Neumann, E.-R., 1994. The Oslo rift: P–T relations and lithospheric structure. Tectonophysics 240, 159–172.
Neumann, E.-R., Pallesen, S., Andresen, P., 1986. Mass estimates of cumulates and residues after anatexis in the Oslo Graben. J. Geophys. Res. 91, 11629–11640.
Neumann, E.-R., Tilton, G.R., Tuen, E., 1988. Sr, Nd and Pb isotope geochemistry of the Oslo rift igneous province, southeast Norway. Geochim. Cosmochim. Acta 52, 1997–2007.
Neumann, E.-R., Sundvoll, B., Øverli, P.E., 1990. A mildly depleted upper mantle beneath southeast Norway: evidence from basalts in the Permo-Carboniferous Oslo rift. In: Neumann, E.-R. (Ed.), Rift Zones in the Continental Crust of Europe- Geophysical, Geological and Geochemical Evidence: Oslo-Horn Graben. Tectonophysics, vol. 178, pp. 89–107.
Neumann, E.-R., Olsen, K.H., Baldridge, W.S., Sundvoll, B., 1992. The Oslo rift: a review. Tectonophysics 208, 1–18.
Neumann, E.-R., Wulff-Pedersen, E., Simonsen, S.L., Pearson, N.J., Mitjavila, J., Martí, J., 1999. Evidence for fractional crystallization of periodically refilled magma chambers in Tenerife, Canary Islands. J. Petrol. 40, 1089–1123.
Øverli, P.-E., 1985. A stratigraphic and petrological investigation of the Horten basalts, B1-level, the southern part of the Oslo Region (in Norwegian). Cand. real. thesis, University of Oslo, 108 pp.
Ramberg, I.B., 1976. Gravimetry interpretation of the Oslo Graben and associated igneous rocks. Nor. Geol. Unders. 325, 1–194.
Ramberg, I.B., Larsen, T.B., 1978. Tectonomagmatic evolution. In: Dons, J.A., Larsen, B.T. (Eds.), The Oslo Paleorift. A Review and Guide to Excursions. Nor. Geol. Unders., vol. 337, pp. 105–124.
Ramberg, I.B., Smithson, S.B., 1971. Gravity interpretation of the Southern Oslo Graben and adjacent Precambrian rocks. Tectonophysics 11, 419–431.
Robinson, J.A.C., Wood, B.J., Blundy, J.D., 1998. The beginning of melting of fertile and depleted peridotite at 1.5 GPa. Earth Planet. Sci. Lett. 155, 97–111.
Schmidt, K.H., Bottazzi, P., Vannucci, R., Mengel, K., 1999. Trace element partitioning between phlogopite, clinopyroxene and leucite lamproite melt. Earth Planet. Sci. Lett. 168, 287–299.
Schou-Jensen, E., Neumann, E.-R., 1988. Volcanic rocks on Jeløya, central Oslo Region: the mafic lavas. Nor. Geol. Tidsskr. 68, 289–308.
Segalstad, T.V., 1979. Petrology of the Skien basaltic rocks, southwestern Oslo Region, Norway. Lithos 12, 221–239.
Sigmarsson, O., Carn, S., Carracedo, J.C., 1998. Systematics of U-series nuclides in primitive lavas from the 1730–36 eruption on Lanzarote, Canary Islands, and implications for the role of garnet pyroxenite during oceanic basalt formation. Earth Planet. Sci. Lett. 162, 137–151.
Sigurdsson, I.A., Steinthorsson, S., Grönvold, K., 2000. Calcium-rich melt inclusions in Cr-spinels from Borgarhraun, northern Iceland. Earth Planet. Sci. Lett. 183, 15–26.
Stein, M., Hofmann, A.W., 1994. Mantle plumes and episodic crustal growth. Nature 372, 63–68.
Sun, S.S., McDonough, W.F., 1989. Chemical and isotopic systematics of ocean basalts: implications for mantle composition and processes. In: Saunders, A.D., Norry, M.J. (Eds.), Magmatism in the Ocean Basins. Spec. Publ.-Geol. Soc. London, vol. 42, pp. 313–345.
Sundvoll, B.A., Larsen, B.T., 1994. Architecture and early evolution of the Oslo rift. Tectonophysics 240, 173–189.
Sundvoll, B.A., Neumann, E.-R., Larsen, B.T., Tuen, E., 1990. Age relations among Oslo rift magmatic rocks: implications for tectonic and magmatic modelling. Tectonophysics 189, 67–87.
Tiepolo, M., Vannucci, R., Bottazzi, P., Oberti, R., Zanetti, A., Foley, S., 2000. Partitioning of rare earth elements, Y, Th, U, and Pb between pargasite, kaersutite, and basanite to trachyte melts: implications for percolated and veined mantle. Geochemistry, Geophysics, Geosystems 1, Paper number 2000GC000064.
Tollefsrud, J.I., 1987. A stratigraphic and petrological investigation of the Holmestrand basalts, B1-level, southern Oslo Region (in Norwegian). Cand. real. thesis, University of Oslo, 133 pp.
Weaver, B.L., 1991. Trace element evidence for the origin of ocean-island basalts. Geology 19, 123–126.
Wessel, P., Husebye, E.S., 1987. The Oslo Graben gravity high and taphrogenesis. Tectonophysics 142, 15–26.
Wilson, M., Lyashkevich, Z.M., 1996. Magmatism and the geodynamics of rifting of the Pripyat–Dnieper–Donets rift, East European Platform. Tectonophysics 268, 65–81.
Wilson, M., Rosenbaum, J.M., Dunworth, E.A., 1995. Melilitites: partial melts of the thermal boundary layer? Contrib. Mineral Petrol. 119, 181–196.
Witt-Eickschen, G., Harte, B., 1994. Distribution of trace elements between amphibole and clinopyroxene from mantle peridotites of the Eifel (Western Germany); an ion-microprobe study. Chem. Geol. 117, 235–250.
Woodland, A.B., Kornprobst, J., McPherson, E., Bodinier, J.-L., Menzies, M.A., 1996. Metasomatic interactions in the lithospheric mantle: petrologic evidence from the Lherz massif, French Pyronees. Chem. Geol. 134, 83–112.
Zindler, A., Hart, S.R., 1986. Chemical geodynamics. Annu. Rev. Earth Planet. Sci. 14, 493–571.